J. Math. Fluid Mech. (2022) 24:97

1422-6928/22/040001-27
https://doi.org/10.1007/s00021-022-00720-4

Journal of Mathematical Fluid Mechanics

Kinetic-Energy Instability of Flows With Slip Boundary Conditions

Ingeborg G. Gjerde and L. Ridgway Scott

Communicated by O. Pironneau

Abstract. We utilize the notion of kinetic energy instability due to Reynolds and Orr to examine instability of steady flow past a bluff body subject to slip boundary conditions with friction. We consider in detail flow past a cylinder. One such solution is given by potential flow with a particular friction coefficient. We compute numerically the eigenproblem determining the most unstable modes. These correspond to modes previously observed in dynamic simulations, confirming the previous observations.

The method of Reynolds and Orr [34] has recently been used [33] to determine the most unstable mode for Couette flow. We extend this analysis to flow around a cylinder, including a slip boundary condition due to Navier [25]. It should be noted that the slip boundary conditions are deduced from the weak formulation, in the weak sense.

Serrin [34] used techniques that he attributed to Reynolds and Orr separately to prove stability of fluid flow. The method is called the kinetic energy stability criterion in [31]. It provides an exact, nonlinear instability criterion that rigorously predicts exponential growth of perturbations, as opposed to the linear instability criterion that is widely used [4,14,20–22,28,31]. Linear stability theory predicts stability of Couette flow [1,30] for all Reynolds numbers, contrary to experimental and computational evidence [7,26,37,38]. A detailed comparison of the two approaches to instability is given in [33]. One conclusion is that any instability found by linear instability theory will also be found by the nonlinear Reynolds–Orr kinetic energy instability theory, so the latter is significantly more general as well as being more rigorous.

A summary of the history of the slip condition is given in the appendix of Goldstein's book [13, pages 676–679], in the introduction to [19], and in [25]. The latter reference describes the effects caused by Stokes advocating a universal no-slip condition ($\mathbf{u} = 0$ on solid boundaries), as well as the original insight of Navier regarding slip conditions (3) and friction. We expect that, as the Reynolds number increases, the flow profile should tend to a solution of the Euler equations [6,8,39,40], for which the slip boundary condition is appropriate and the flow in simple domains is plug-like. On the other hand, as the friction coefficient tends to infinity, the Navier condition converges to the Stokes condition. Thus the Navier slip (friction) condition generalizes the Stokes (Dirichlet) condition and gives something more physically rigorous.

The Stokes no-slip condition is a good approximation in many cases, but it introduces a hard constraint that can be a computational impediment for some flows. Here we are using terminology from optimization: the Navier condition can be thought of as relaxing the Stokes constraint $\mathbf{u} = 0$. Variationally, we work in a larger, less constrained space.

By contrast, the Navier boundary condition expresses a balance between the amount of slip and the shear stress. Thus there is no need to over-refine near boundaries. Having a constraint on the normal component of flow is only an orientational restriction: fluids flow in only one direction at each point. But the Stokes condition forces the flow velocity to vanish, and full resolution may require substantial mesh refinement near the constraint region.

Thus we see that the Navier slip-with-friction boundary condition is both physically more accurate [25,27,42] and computationally easier to work with. By taking the friction coefficient arbitrarily large, we can recover the Stokes no-slip condition, so nothing is lost in using the more general Navier condition. Surprisingly, we find that flow instabilities (both the Reynolds numbers at which they are activated and the form of the unstable fluid velocity mode) appear to converge at rather modest friction coefficient values.

We also find that there is a convergence of the instabilities regarding increasing Reynolds number (decreasing viscosity). We derive rigorously an approximate scaling rule regarding the critical viscosities at which instabilities get activated, and we observe computationally strong similarity of the corresponding flow modes. Thus we can predict with some confidence the form of the most unstable modes for even larger flow speeds than our current computations support. The most unstable modes are supported downstream of the cylinder, in concert with what was observed in [17]. Thus we provide support for the observations in [17] with both mathematical theory and extensive computations.

To incorporate the Navier slip boundary condition, we modify here the energy instability criterion for viscous, incompressible fluid flow [31,33,34] to allow slip boundary conditions. We focus on flow past a cylinder since it is both a very simple flow geometry and also a very well studied problem [43,44]. However, our methodology easily extends to more general geometries.

One striking result is that potential flow around a cylinder is an exact solution of the Navier-Stokes equations when a relation holds between the kinematic viscosity and the Navier friction coefficient. This means that there is no boundary layer for such a solution. For these solutions and others, we compute the most unstable modes in both two and three dimensions.

Our results support a dramatic shift in thinking about computational fluid dynamics. As advocated in [17], there is a great deal of fluid flow that can be described as laminar base flows modified by instabilities. Such a view can have substantial impact not only on simulation of aircraft flight, but also in modeling abnormalities in flow of bodily fluids, in designing energy generation systems, novel transportation systems, and much more.

1. Base Flow Equations

Suppose that $(\mathbf{u}, p)$ is a weak solution of the Navier-Stokes equations in a bounded, Lipschitz domain $\Omega \subset \mathbb{R}^d$ ($d = 2$ or 3) containing an obstacle with boundary $\Gamma \subset \partial\Omega$:

$$\begin{aligned} &\mathbf{u}_t - \nu\Delta\mathbf{u} + \mathbf{u}\cdot\nabla\mathbf{u} + \nabla p = \mathbf{0} \text{ in } \Omega, \\ &\nabla\cdot\mathbf{u} = 0 \text{ in } \Omega, \end{aligned} \tag{1}$$

where ν is a nondimensional parameter related to the kinematic viscosity, together with boundary conditions

$$\mathbf{u} = \mathbf{g} \text{ on } \partial\Omega\backslash\Gamma, \quad \mathbf{u}\cdot\mathbf{n} = 0 \text{ on } \Gamma, \tag{2}$$

together with Navier's slip condition [12,25] linking tangential velocity and the shear stress on Γ:

$$\beta\,\mathbf{u}\cdot\boldsymbol{\tau}_i = -\nu\,\mathbf{n}^t(\nabla\mathbf{u} + \nabla\mathbf{u}^t)\boldsymbol{\tau}_i, \quad i = 1, 2, \tag{3}$$

where $\boldsymbol{\tau}_i$ are orthogonal tangent vectors and β is the friction coefficient. We assume initial conditions $\mathbf{u}(\mathbf{x}, 0) = \mathbf{u}_0(\mathbf{x})$ for $\mathbf{x} \in \Omega$. The equations hold in a domain Ω and for $t \in [0, T]$. We assume that $\mathbf{g} = \mathbf{0}$ on Γ for simplicity.

The flow is inside Ω but outside Γ which represents some obstacle, such as a cylinder. The theory behind the Navier-Stokes equations is well known [23,36], except that the slip condition is somewhat novel. Define the spaces V and H by [36]

$$\begin{aligned} V &= \left\{\mathbf{v} \in H^1(\Omega)^d \ : \ \nabla\cdot\mathbf{v} = 0 \text{ in } \Omega, \quad \mathbf{v} = \mathbf{0} \text{ on } \partial\Omega\backslash\Gamma, \quad \mathbf{v}\cdot\mathbf{n} = 0 \text{ on } \Gamma\right\}, \\ H &= \left\{\mathbf{v} \in L^2(\Omega)^d \ : \ \nabla\cdot\mathbf{v} = 0 \text{ in } \Omega\right\}. \end{aligned} \tag{4}$$

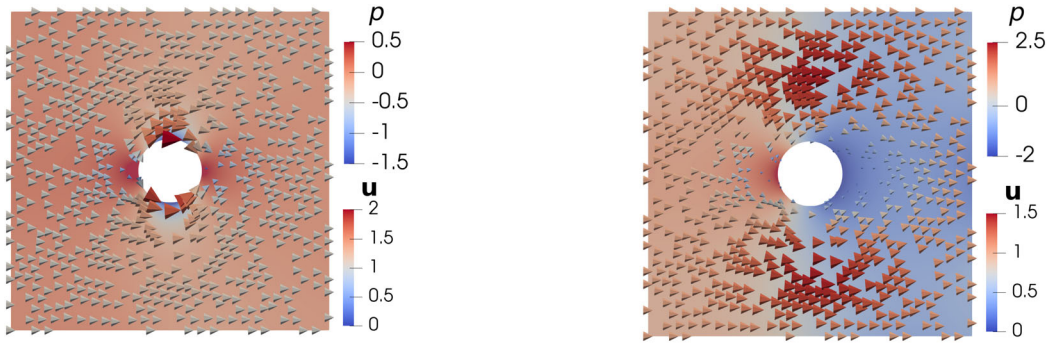

(a) $\beta = -2$ **(b)** $\beta = 2$

FIG. 1. Solution of the Navier-Stokes equations (1,2,3) for $\nu = 1$ with **(a)** $\beta = -2$ and **(b)** $\beta = 2$. The computation was done in a box of dimensions 5×5, and the cylinder of radius 1 is centered vertically and placed one-third of the way from the inflow (left) side of the box. Dirichlet/Stokes conditions on the boundary of the box were given by the potential flow solution

We view V as a Hilbert space with the $H^1(\Omega)$ norm. In [36, Theorem 3.1, page 282], it is proved that, for any $\mathbf{u}_0 \in H$, there is some $T > 0$ such that a solution of the system (1—2) together with Dirichlet boundary conditions on Γ satisfying

$$\mathbf{u} \in L^2(0, T; V) \cap L^\infty(0, T; H), \tag{5}$$

and $\mathbf{u}$ is weakly continuous from $[0, T]$ into H. It is explained in [6, Theorem 2.3] how to extend such results to slip boundary conditions.

With such weak assumptions on the initial data, we cannot guarantee uniqueness of solutions. But we will see that instability depends only on the initial data, so our results apply to all solutions.

The Navier boundary condition simplifies variationally, as we now recall. The coefficient β can vary in space to match the geometry of Γ appropriately. It also would be possible to have different β's for each tangential direction $\boldsymbol{\tau}_i$. In the case of the cylinder, we can choose one tangent direction parallel to the axis of the cylinder, and the other tangent direction parallel to the main flow direction. It is conceivable that for some materials, different β_i would be appropriate.

Define

$$\mathcal{D}(\mathbf{v}) = \nabla \mathbf{v} + \nabla \mathbf{v}^t.$$

In [6,12], it is shown that the variational formulation for the time-dependent problem is

$$(\mathbf{u}_t, \mathbf{v}) + \frac{\nu}{2}(\mathcal{D}(\mathbf{u}), \mathcal{D}(\mathbf{v})) + (\mathbf{u} \cdot \nabla \mathbf{u}, \mathbf{v}) + \oint_{\partial\Omega} \beta \sum_{i=1}^{d-1} (\boldsymbol{\tau}_i \cdot \mathbf{v})(\boldsymbol{\tau}_i \cdot \mathbf{u})\, ds = 0 \tag{6}$$

for all $\mathbf{v} \in V$, since $(p, \nabla \cdot \mathbf{v}) = 0$ for $\mathbf{v} \in V$. The tangent vectors $\boldsymbol{\tau}_i$ were defined subsequent to (3). The boundary term can be written in coordinate-free form by introducing the tangent space T to Γ, and the projection P_T onto the tangent space. Then

$$\sum_{i=1}^{d-1} (\boldsymbol{\tau}_i \cdot \mathbf{v})(\boldsymbol{\tau}_i \cdot \mathbf{u}) = (P_T \mathbf{v}) \cdot (P_T \mathbf{u}). \tag{7}$$

We see that, in general, β could be a matrix, with the boundary term involving $(P_T \mathbf{v})^t \beta (P_T \mathbf{u})$, but we will stick here to the scalar case.

2. Flow Instability

Similarly, suppose that $(\mathbf{w}, q)$ is another solution of the Navier-Stokes equations

$$\begin{aligned} &\mathbf{w}_t - \nu\Delta\mathbf{w} + \mathbf{w}\cdot\nabla\mathbf{w} + \nabla q = \mathbf{0} \text{ in } \Omega\times[0,T],\\ &\nabla\cdot\mathbf{w} = 0 \text{ in } \Omega\times[0,T], \quad \mathbf{w} = \mathbf{g} \text{ on } \partial\Omega\backslash\Gamma\times[0,T], \quad \mathbf{w}\cdot\mathbf{n} = 0 \text{ on } \Gamma\times[0,T],\\ &\beta\mathbf{w}\cdot\boldsymbol{\tau}_i + \nu\mathbf{n}^t\mathcal{D}(\mathbf{w})\boldsymbol{\tau}_i = 0, \quad i = 1,\dots,d-1, \text{ on } \Gamma\times[0,T], \end{aligned} \tag{8}$$

with friction coefficient β and with initial conditions $\mathbf{w}(\mathbf{x},0) = \mathbf{w}_0(\mathbf{x})$ for $\mathbf{x}\in\Omega$. We assume $\mathbf{w}_0 \in H$, where H is the space defined in (4). Like $\mathbf{u}$ in (5), we have

$$\mathbf{w} \in L^2(0,T;V)\cap L^\infty(0,T;H), \tag{9}$$

and $\mathbf{w}$ is weakly continuous from $[0,T]$ into H.

Suppose that $\mathbf{u}$ and $\mathbf{w}$ differ slightly at $t=0$: $\mathbf{v}_0 = \mathbf{u}_0 - \mathbf{w}_0 \neq \mathbf{0}$.

Definition 2.1. Suppose that $\mathbf{v}_0 \in H$. Define the *kinetic energy* difference

$$\mathcal{E}(t) = \int_\Omega |\mathbf{u}(t) - \mathbf{w}(t)|^2\, d\mathbf{x}, \tag{10}$$

where $\mathbf{w}$ is defined by (8) with $\mathbf{w}(0) = \mathbf{u}_0 - \mathbf{v}_0$. We say that the flow $\mathbf{u}$ is *kinetic energy unstable* at $t=0$ due to the perturbation $\mathbf{v}_0$ for viscosity ν and friction coefficient β if

$$\frac{d}{dt}\mathcal{E}(0) > 0. \tag{11}$$

If $\mathcal{E}'(0) \le 0$ for all $\mathbf{v}_0 \in H$, then we say that the flow $\mathbf{u}$ is *kinetic energy stable* at $t=0$.

The terminology *kinetic energy (un)stable* is derived from [31, Section 5.6]. We will frequently drop the modifier 'kinetic' and just say *energy (un)stable*.

The regularity required to make $\mathcal{E}$ differentiable at $t=0$ will be discussed in section 2.5.

2.1. Interpreting the Energy Instability Condition

If we define $\mathbf{v}$ for all time by

$$\mathbf{v} = \mathbf{u} - \mathbf{w},$$

then we see that the condition (11) is equivalent to

$$\frac{d}{dt}\int_\Omega |\mathbf{v}|^2\, d\mathbf{x} > 0 \tag{12}$$

at $t=0$. By subtracting $\mathbf{w}$ from $\mathbf{u}$, we have

$$\mathbf{v} \in L^2(0,T;V)\cap L^\infty(0,T;H), \tag{13}$$

with $\mathbf{v}$ weakly continuous from $[0,T]$ into H, and we see that $\mathbf{v}$ solves the equations

$$\begin{aligned} &\mathbf{v}_t - \nu\Delta\mathbf{v} + \big(\mathbf{u}\cdot\nabla\mathbf{u} - \mathbf{w}\cdot\nabla\mathbf{w}\big) + \nabla o = \mathbf{0} \text{ in } \Omega\times[0,T],\\ &\nabla\cdot\mathbf{v} = 0 \text{ in } \Omega\times[0,T], \quad \mathbf{v} = \mathbf{0} \text{ on } \partial\Omega\backslash\Gamma\times[0,T], \quad \mathbf{v}\cdot\mathbf{n} = 0 \text{ on } \Gamma\times[0,T],\\ &\beta\mathbf{v}\cdot\boldsymbol{\tau}_i + \nu\mathbf{n}^t\mathcal{D}(\mathbf{v})\boldsymbol{\tau}_i = 0, \quad i = 1,\dots,d-1, \text{ on } \Gamma\times[0,T], \end{aligned} \tag{14}$$

where $o = p - q$ and $\mathbf{v}(t=0) = \mathbf{v}_0 = \mathbf{u}_0 - \mathbf{w}_0$. We expand the nonlinear terms as follows:

$$\begin{aligned} \mathbf{u}\cdot\nabla\mathbf{u} - \mathbf{w}\cdot\nabla\mathbf{w} &= \mathbf{u}\cdot\nabla\mathbf{u} - \mathbf{u}\cdot\nabla\mathbf{w} + \mathbf{u}\cdot\nabla\mathbf{w} - \mathbf{w}\cdot\nabla\mathbf{w} = \mathbf{u}\cdot\nabla\mathbf{v} + \mathbf{v}\cdot\nabla\mathbf{w}\\ &= \mathbf{u}\cdot\nabla\mathbf{v} + \mathbf{v}\cdot\nabla(\mathbf{u}-\mathbf{v}) = \mathbf{u}\cdot\nabla\mathbf{v} + \mathbf{v}\cdot\nabla\mathbf{u} - \mathbf{v}\cdot\nabla\mathbf{v}. \end{aligned} \tag{15}$$

Thus the first equation in (14) becomes

$$\mathbf{v}_t - \nu\Delta\mathbf{v} + \big(\mathbf{u}\cdot\nabla\mathbf{v} + \mathbf{v}\cdot\nabla\mathbf{u} - \mathbf{v}\cdot\nabla\mathbf{v}\big) + \nabla o = \mathbf{0} \text{ in } \Omega\times[0,T]. \tag{16}$$

Therefore we can determine if an instability occurs by solving (16). We will see that we can determine it more simply.

2.2. An Exact Nonlinear Bound for Kinetic Energy

Subtracting the variational formulations (6) for $\mathbf{u}$ and $\mathbf{w}$, and choosing $\mathbf{v} = \mathbf{u} - \mathbf{w}$ as test function, we get

$$\begin{aligned} \frac{1}{2}\frac{d}{dt}\int_\Omega |\mathbf{v}|^2\,d\mathbf{x} + \frac{\nu}{2}\int_\Omega |\mathcal{D}(\mathbf{v})|^2\,d\mathbf{x} + \oint_\Gamma \beta\,|P_T\mathbf{v}|^2\,ds \\ + \big(c(\mathbf{u},\mathbf{v},\mathbf{v}) + c(\mathbf{v},\mathbf{u},\mathbf{v}) - c(\mathbf{v},\mathbf{v},\mathbf{v})\big) = 0, \end{aligned} \tag{17}$$

where the projection P_T onto the tangent space is defined in (7),

$$c(\mathbf{u},\mathbf{v},\mathbf{w}) = \int_\Omega (\mathbf{u}\cdot\nabla\mathbf{v})\cdot\mathbf{w}\,d\mathbf{x}, \quad \forall\ \mathbf{u},\mathbf{v},\mathbf{w} \in H^1(\Omega)^d \quad [23,\ \textit{Lemme}\ 6.1], \tag{18}$$

and the boundary integral on Γ results from the Navier slip boundary condition (3). It is well known [32, Section 20.1.2], that

$$c(\mathbf{u},\mathbf{v},\mathbf{w}) = -c(\mathbf{u},\mathbf{w},\mathbf{v}) + \oint_{\partial\Omega} \mathbf{u}\cdot\mathbf{n}\,(\mathbf{v}\cdot\mathbf{w})\,ds.$$

For $\mathbf{v} \in V$, we thus have $c(\mathbf{u},\mathbf{v},\mathbf{v}) = 0$, and $c(\mathbf{v},\mathbf{v},\mathbf{v}) = 0$, in (17), since $\mathbf{u}\cdot\mathbf{n} = 0$ on Γ and $\mathbf{v} = \mathbf{0}$ on $\partial\Omega\backslash\Gamma$. Moreover

$$c(\mathbf{v},\mathbf{u},\mathbf{v}) = \int_\Omega (\mathbf{v}\cdot\nabla\mathbf{u})\cdot\mathbf{v}\,d\mathbf{x} = \int_\Omega \mathbf{v}^t(\nabla\mathbf{u})\mathbf{v}\,d\mathbf{x} = \frac{1}{2}\int_\Omega \mathbf{v}^t\big(\nabla\mathbf{u} + \nabla\mathbf{u}^t\big)\mathbf{v}\,d\mathbf{x}.$$

Thus we find

$$\frac{1}{2}\frac{d}{dt}\int_\Omega |\mathbf{v}|^2\,d\mathbf{x} = -\frac{\nu}{2}\int_\Omega |\mathcal{D}(\mathbf{v})|^2\,d\mathbf{x} - \oint_\Gamma \beta\,|P_T\mathbf{v}|^2\,ds - \frac{1}{2}\int_\Omega \mathbf{v}^t(\nabla\mathbf{u} + \nabla\mathbf{u}^t)\mathbf{v}\,d\mathbf{x}. \tag{19}$$

The kinetic energy relation (19) is similar to what is found in [34, (4)] and [31, Section 5.6.1]. For $\mathbf{v} \in V$, we have $\mathbf{v}\cdot\mathbf{n} = 0$ on Γ, so we have $\mathbf{v} = P_T\mathbf{v}$ in the boundary term in (19). However, we prefer to keep the projection explicit as in the numerical approximation using Nitsche's method we will relax the requirement $\mathbf{v}\cdot\mathbf{n} = 0$.

For all $\mathbf{x} \in \Omega$ and $t \in [0,T]$, the matrix $B(\mathbf{x},t)$ defined by

$$B(\mathbf{x},t) = \nabla\mathbf{u}(\mathbf{x},t) + \nabla\mathbf{u}(\mathbf{x},t)^t \tag{20}$$

is symmetric and has trace zero. Thus B may have eigenvalues of both signs, and in particular it might happen that

$$-\frac{\nu}{2}\int_\Omega |\mathcal{D}(\mathbf{v}_0)|^2\,d\mathbf{x} - \oint_\Gamma \beta\,|P_T\mathbf{v}_0|^2\,ds - \frac{1}{2}\int_\Omega \mathbf{v}_0^t\big(\nabla\mathbf{u}_0 + \nabla\mathbf{u}_0^t\big)\mathbf{v}_0\,d\mathbf{x} > 0,$$

in which case $\|\mathbf{v}\|_{L^2(\Omega)}$ would initially increase. This suggests a criterion for stability.

2.3. Energy Instability Criterion

Now we assume that $\mathbf{u}_0 \in H^1(\Omega)^d$. Recall the definition (4) of the space V. If there exists $\mathbf{v}_0 \in V$ that

$$-\frac{1}{2}\int_\Omega \mathbf{v}_0^t(\nabla\mathbf{u}_0 + \nabla\mathbf{u}_0^t)\mathbf{v}_0\,d\mathbf{x} > \frac{\nu}{2}\int_\Omega |\mathcal{D}(\mathbf{v}_0)|^2\,d\mathbf{x} + \oint_\Gamma \beta\,|P_T\mathbf{v}_0|^2\,ds, \tag{21}$$

then (19) implies that the flow is energy unstable at $t = 0$, leading to the following criterion for instability.

Theorem 2.1. *The flow* $\mathbf{u}$ *that is the unique solution of the system (1—3) is energy unstable at* $t = 0$ *for viscosity* ν *and friction coefficient* β *if and only if*

$$\begin{aligned} &-\inf_{\mathbf{0}\neq\mathbf{v}\in V} \frac{\frac{1}{2}\int_\Omega \mathbf{v}^t(\nabla\mathbf{u}_0+\nabla\mathbf{u}_0^t)\mathbf{v}\,d\mathbf{x}}{\frac{1}{2}\nu\int_\Omega|\mathcal{D}(\mathbf{v})|^2\,d\mathbf{x}+\oint_\Gamma\beta\,|P_T\mathbf{v}|^2\,ds} \\ &\quad=\sup_{\mathbf{0}\neq\mathbf{v}\in V} -\frac{\frac{1}{2}\int_\Omega \mathbf{v}^t(\nabla\mathbf{u}_0+\nabla\mathbf{u}_0^t)\mathbf{v}\,d\mathbf{x}}{\frac{1}{2}\nu\int_\Omega|\mathcal{D}(\mathbf{v})|^2\,d\mathbf{x}+\oint_\Gamma\beta\,|P_T\mathbf{v}|^2\,ds} > 1. \end{aligned} \tag{22}$$

If (22) holds, it means there is some $\mathbf{v}_0$ that could lead to instability. What we need to show is that it is smooth enough. We postpone complete details to sect. 3.4.

On the other hand, if by chance

$$-\inf_{\mathbf{0}\neq\mathbf{v}\in V} \frac{\frac{1}{2}\int_\Omega \mathbf{v}^t(\nabla\mathbf{u}_0+\nabla\mathbf{u}_0^t)\mathbf{v}\,d\mathbf{x}}{\frac{1}{2}\nu\int_\Omega|\mathcal{D}(\mathbf{v})|^2\,d\mathbf{x}+\oint_\Gamma\beta\,|P_T\mathbf{v}|^2\,ds} \le 1,$$

then

$$\frac{d}{dt}\int_\Omega|\mathbf{v}|^2\,d\mathbf{x}\le 0$$

for all $\mathbf{v}_0\in V$, and thus the flow is energy stable.

Therefore Definition 2.1 and (22) are equivalent. In [33], (22) was taken as the definition of kinetic energy instability, but we are using Definition 2.1 as it is more transparent.

2.4. Most Unstable Mode

A central result of the paper is that the parameter λ, defined by

$$\lambda=\inf_{\mathbf{0}\neq\mathbf{v}\in V}\frac{\frac{1}{2}\int_\Omega \mathbf{v}^t(\nabla\mathbf{u}_0+\nabla\mathbf{u}_0^t)\mathbf{v}\,d\mathbf{x}}{\frac{1}{2}\int_\Omega\nu|\mathcal{D}(\mathbf{v})|^2\,d\mathbf{x}+\oint_\Gamma\beta\,|P_T\mathbf{v}|^2\,ds}, \tag{23}$$

is [33] a generalized eigenvalue for the following variational equation, to find $\mathbf{v}_\lambda\in V$ such that

$$\frac{\nu}{2}\int_\Omega\mathcal{D}(\mathbf{v}_\lambda):\mathcal{D}(\mathbf{z})\,d\mathbf{x}+\oint_\Gamma\beta P_T\mathbf{v}_\lambda\cdot P_T\mathbf{z}\,ds=\lambda^{-1}\int_\Omega\big(B\mathbf{v}_\lambda\big)\cdot\mathbf{z}\,d\mathbf{x}\quad\forall\mathbf{z}\in V, \tag{24}$$

where $B=\frac{1}{2}\big(\nabla\mathbf{u}_0+\nabla\mathbf{u}_0^t\big)$. If (22) holds, then $\lambda<-1$.

We can clarify this eigenproblem by writing the following variational problem: given $\mathbf{w}\in V$, find $\mathbf{v}\in V$ such that

$$\frac{\nu}{2}\int_\Omega\mathcal{D}(\mathbf{v}):\mathcal{D}(\mathbf{z})\,d\mathbf{x}+\oint_\Gamma\beta P_T\mathbf{v}\cdot P_T\mathbf{z}\,ds=\int_\Omega\big(B\mathbf{w}\big)\cdot\mathbf{z}\,d\mathbf{x}\quad\forall\mathbf{z}\in V. \tag{25}$$

We will discuss the coercivity of this problem in sect. 3.1. Define the operator $K:V\to V$ by $K\mathbf{w}=\mathbf{v}$. Then (24) is equivalent to $K\mathbf{v}=\lambda\mathbf{v}$. Thus the λ's in (24) correspond to the eigenvalues of the operator K. We can think of K as extended to a mapping on $L^2(\Omega)^d$, and it is a compact operator in this setting. Coercivity in (25) implies that K is invertible, so $\lambda\neq 0$. Thus the notation $\mathbf{v}_\lambda$ does not conflict with the notation $\mathbf{v}_0$ for the initial data.

We will identify all eigenfunctions with a negative corresponding eigenvalue as a potential unstable mode. Our justification for this is the scaling law presented in Sect. 3.3, where we show that λ scales with the Reynolds number. Thus, all modes with $\lambda<0$ will eventually become unstable as the Reynolds number increases.

We collect the above analysis in the following.

Theorem 2.2. *Let* λ *be the most negative eigenvalue for the equation (24), where* $B=\frac{1}{2}\big(\nabla\mathbf{u}_0+\nabla\mathbf{u}_0^t\big)$. *If* $\lambda\ge-1$, *the flow starting with* $\mathbf{u}(0)=\mathbf{u}_0$ *is energy stable at* $t=0$. *If* $\lambda<-1$, *the flow* $\mathbf{u}$ *is energy unstable at* $t=0$, *with* $\mathbf{v}_\lambda$ *in (24) being the most unstable mode.*

2.5. Regularity Requirements

We can now explain the regularity requirements for energy instability determination. We have seen that (11) and (21) are equivalent. For $\mathbf{u}_0$, $\mathbf{v}_0 \in H^1(\Omega)^d$, the terms in (21) are all well defined. Thus the energy instability definition applies for all perturbations $\mathbf{v}_0 \in V$ and for all initial flow velocities $\mathbf{u}_0 \in V$. But that is not to say that the L^2 difference $\mathcal{E}$ is really increasing at $t = 0$. If $\mathbf{u}_0$ and $\mathbf{v}_0$ are a bit smoother, then regularity results for Navier–Stokes (see [36, Theorem 3.7] or [6, Theorem 2.3]) show that the time derivative of $\mathcal{E}$ is in $L^\infty(0,T)$ for some $T > 0$, as follows. Define

$$W = \left\{ \mathbf{u} \in V \cap H^2(\Omega)^d \ : \ (3) \text{ holds on } \Gamma \right\}.$$

In [6, Theorem 2.3], it is proved that, for some $T > 0$, there is a unique solution of the system (1—3) satisfying

$$\mathbf{u} \in L^2(0,T;V) \cap L^\infty(0,T;L^2(\Omega)), \qquad \mathbf{u}_t \in L^2(0,T;V) \cap L^\infty(0,T;L^2(\Omega)), \tag{26}$$

provided $\mathbf{u}_0 \in W$.

If we take one of the eigenmodes $\mathbf{v}_\lambda$ of (24) as initial perturbation, then this will have extra smoothness and (as we show in sect. 3.4) exponential growth will occur. But for general non-smooth perturbations satisfying (21), we are not able to predict growth in time of $\mathcal{E}$. It is beyond the scope of this paper to consider such pathological cases even though we recognize that they may be of significant interest.

3. The Eigenproblem

We give some properties of the eigenproblem (24). To begin with, we give a coercivity result that will be used subsequently.

3.1. Coercivity

Due to the boundary condition on $\partial\Omega\backslash\Gamma$, there is a Poincaré inequality [32, (30.28)] of the form

$$\int_\Omega |\mathbf{v}|^2 \, d\mathbf{x} \le C_b \left(\frac{1}{2} \int_\Omega |\mathcal{D}(\mathbf{v})|^2 \, d\mathbf{x} + \oint_\Gamma b \, |P_T \mathbf{v}|^2 \, ds \right) \quad \forall \mathbf{v} \in V, \tag{27}$$

at least for $|b|$ sufficiently small if $b < 0$. In particular, we take C_b to be the smallest positive constant such that (27) holds.

In particular, $C_0 < \infty$ exists for $b = 0$ just using the boundary conditions on $\partial\Omega\backslash\Gamma$. Define

$$V_0 = \left\{ \mathbf{v} \in H^1(\Omega)^d \ : \ \mathbf{v} = 0 \text{ on } \partial\Omega \right\},$$

observe that $V \subset V_0$, and apply Poincaré's inequality [3, (5.3.3)] on V_0.

The constant C_b depends on Ω and Γ, as well as b. However, we imagine fixing Ω and Γ and varying b, so we have made the dependence explicit. The form of the dependence on b is not obvious, but it is monotone, as we now show. We can show that

$$C_b \le C_{b'} \quad \text{if } \ b' \le b, \tag{28}$$

as follows. Our definition of C_b as the smallest constant satisfying (27) is equivalent to

$$C_b = \sup_{\mathbf{0} \ne \mathbf{v} \in V} \frac{\int_\Omega |\mathbf{v}|^2 \, d\mathbf{x}}{\frac{1}{2} \int_\Omega |\mathcal{D}(\mathbf{v})|^2 \, d\mathbf{x} + \oint_\Gamma b \, |P_T \mathbf{v}|^2 \, ds}. \tag{29}$$

Then for $b' \leq b$,

$$\begin{aligned} \int_\Omega |\mathbf{v}|^2 \, d\mathbf{x} &\leq C_{b'} \left(\frac{1}{2} \int_\Omega |\mathcal{D}(\mathbf{v})|^2 \, d\mathbf{x} + \oint_\Gamma b' |P_T \mathbf{v}|^2 \, ds \right) \\ &\leq C_{b'} \left(\frac{1}{2} \int_\Omega |\mathcal{D}(\mathbf{v})|^2 \, d\mathbf{x} + \oint_\Gamma b |P_T \mathbf{v}|^2 \, ds \right) \end{aligned} \tag{30}$$

for all $\mathbf{v} \in V$. Therefore

$$\frac{\int_\Omega |\mathbf{v}|^2 \, d\mathbf{x}}{\frac{1}{2} \int_\Omega |\mathcal{D}(\mathbf{v})|^2 \, d\mathbf{x} + \oint_\Gamma b |P_T \mathbf{v}|^2 \, ds} \leq C_{b'} \tag{31}$$

for all $\mathbf{v} \in V$. Taking the supremum over $\mathbf{v} \in V$ completes the proof that C_b is nonincreasing in b.

In particular, $C_b \leq C_0$ for all $b > 0$. But it is not clear that C_b is strictly decreasing, and in any case, taking b arbitrarily large does not make C_b go to zero. To see this, let C_Z denote

$$C_Z = \sup_{\mathbf{0} \neq \mathbf{v} \in Z} \frac{\int_\Omega |\mathbf{v}|^2 \, d\mathbf{x}}{\frac{1}{2} \int_\Omega |\mathcal{D}(\mathbf{v})|^2 \, d\mathbf{x}},$$

where

$$Z = \left\{ \mathbf{v} \in H^1(\Omega)^d \ : \ \nabla \cdot \mathbf{v} = 0 \text{ in } \Omega, \quad \mathbf{v} = \mathbf{0} \text{ on } \partial\Omega \right\}. \tag{32}$$

This is the Poincaré constant for Ω and Γ with full Dirichlet conditions. But then

$$\begin{aligned} C_Z = \sup_{\mathbf{0} \neq \mathbf{v} \in Z} \frac{\int_\Omega |\mathbf{v}|^2 \, d\mathbf{x}}{\frac{1}{2} \int_\Omega |\mathcal{D}(\mathbf{v})|^2 \, d\mathbf{x}} &= \sup_{\mathbf{0} \neq \mathbf{v} \in Z} \frac{\int_\Omega |\mathbf{v}|^2 \, d\mathbf{x}}{\frac{1}{2} \int_\Omega |\mathcal{D}(\mathbf{v})|^2 \, d\mathbf{x} + \oint_\Gamma b |P_T \mathbf{v}|^2 \, ds} \\ \leq \sup_{\mathbf{0} \neq \mathbf{v} \in V} \frac{\int_\Omega |\mathbf{v}|^2 \, d\mathbf{x}}{\frac{1}{2} \int_\Omega |\mathcal{D}(\mathbf{v})|^2 \, d\mathbf{x} + \oint_\Gamma b |P_T \mathbf{v}|^2 \, ds} &= C_b. \end{aligned} \tag{33}$$

Therefore

$$0 < C_Z \leq C_b \leq C_0 \tag{34}$$

for all $b \geq 0$.

The inequality (27) expresses the coercivity of the bilinear form

$$\frac{1}{2} \int_\Omega \mathcal{D}(\mathbf{u}) : \mathcal{D}(\mathbf{v}) \, d\mathbf{x} + \oint_\Gamma b \, P_T \mathbf{u} \cdot P_T \mathbf{v} \, ds.$$

Coercivity fails if there is a $\mathbf{u} \in V$ and constant b_0 such that

$$\frac{1}{2} \int_\Omega \mathcal{D}(\mathbf{u}) : \mathcal{D}(\mathbf{v}) \, d\mathbf{x} = -b_0 \oint_\Gamma P_T \mathbf{u} \cdot P_T \mathbf{v} \, ds \tag{35}$$

for all $\mathbf{v} \in V$. This is an eigenproblem that we can compute for a given Ω and Γ. Coercivity then holds for $b > -b_0$. Coercivity implies the well-posedness of the eigenproblem (24), and it can have an impact on the choice of eigensolvers.

3.2. Bounds for the Eigenvalues

Recall that $B = \frac{1}{2}(\nabla \mathbf{u}_0 + \nabla \mathbf{u}_0^t)$. Let us now assume that $\nabla \mathbf{u}_0 \in L^\infty(\Omega)$. From Hölder's inequality,

$$\left| \int_\Omega (B\mathbf{v}) \cdot \mathbf{v} \, d\mathbf{x} \right| \leq \sup_{\mathbf{x} \in \Omega} \|\nabla \mathbf{u}_0(\mathbf{x})\|_F \int_\Omega |\mathbf{v}|^2 \, d\mathbf{x},$$

where $\|\nabla \mathbf{u}_0(\mathbf{x})\|_F$ denotes the Frobenius norm of the matrix $\nabla \mathbf{u}_0(\mathbf{x})$. The coercivity bound (27) thus shows that for any $\mathbf{v} \in V$, we have

$$\left| \int_\Omega (B\mathbf{v}) \cdot \mathbf{v} \, d\mathbf{x} \right| \leq C_b \sup_{\mathbf{x} \in \Omega} \|\nabla \mathbf{u}_0(\mathbf{x})\|_F \left(\frac{1}{2} \int_\Omega |\mathcal{D}(\mathbf{v})|^2 \, d\mathbf{x} + \oint_\Gamma b \, |P_T \mathbf{v}|^2 \, ds \right). \tag{36}$$

Any eigenvalue λ of (24) satisfies

$$\begin{aligned}\frac{1}{2}\int_\Omega \mathcal{D}(\mathbf{v}_\lambda):\mathcal{D}(\mathbf{v}_\lambda)\,d\mathbf{x}+\oint_\Gamma \frac{\beta}{\nu}\,P_T\mathbf{v}_\lambda\cdot P_T\mathbf{v}_\lambda\,ds=\frac{1}{\nu\lambda}\int_\Omega (B\mathbf{v}_\lambda)\cdot\mathbf{v}_\lambda\,d\mathbf{x}\\ \le \frac{C_b}{\nu|\lambda|}\sup_{\mathbf{x}\in\Omega}\|\nabla\mathbf{u}_0(\mathbf{x})\|_F\left(\frac{1}{2}\int_\Omega|\mathcal{D}(\mathbf{v}_\lambda)|^2\,d\mathbf{x}+\oint_\Gamma b\,|P_T\mathbf{v}_\lambda|^2\,ds\right)\end{aligned} \tag{37}$$

for any b. Taking $b=\beta/\nu$, dividing by $\frac{1}{2}\int_\Omega|\mathcal{D}(\mathbf{v}_\lambda)|^2\,d\mathbf{x}+\oint_\Gamma b\,|P_T\mathbf{v}_\lambda|^2\,ds$, and multiplying by $|\lambda|$ yields

$$|\lambda|\le\frac{C_{\beta/\nu}}{\nu}\sup_{\mathbf{x}\in\Omega}\|\nabla\mathbf{u}_0(\mathbf{x})\|_F. \tag{38}$$

The constant C_b was defined in (27) and is a coercivity constant that can be computed via an eigenproblem similar to the instability computations.

3.3. Eigenvalue Scaling

We can write the most negative eigenvalue of (24) as $\lambda_{\nu,\beta}$ to emphasize its dependence on the two parameters. For flow around a cylinder with $\beta=-2\nu$, it turns out that $\mathbf{u}_{\nu,-2\nu}=\mathbf{u}_{1,-2}=$ potential flow, for any $\nu>0$, as we show in sect. 4.3. But in general, $\mathbf{u}_{\nu,\beta}\ne\mathbf{u}_{1,\beta/\nu}$, so some care needs to be taken.

It follows from (23) that

$$\nu\lambda_{\nu,\beta}=\lambda_{1,\beta/\nu}, \tag{39}$$

provided that $\mathbf{u}$ does not change as ν and β are varied, as is the case for potential flow with $\beta=-2\nu$. This follows from

$$\begin{aligned}\lambda_{\nu,\beta}&=\inf_{\mathbf{0}\ne\mathbf{v}\in V}\frac{\frac{1}{2}\int_\Omega\mathbf{v}^t(\nabla\mathbf{u}_0+\nabla\mathbf{u}_0^t)\mathbf{v}\,d\mathbf{x}}{\frac{1}{2}\int_\Omega\nu|\mathcal{D}(\mathbf{v})|^2\,d\mathbf{x}+\oint_\Gamma\beta\,|P_T\mathbf{v}|^2\,ds}\\ &=\frac{1}{\nu}\inf_{\mathbf{0}\ne\mathbf{v}\in V}\frac{\frac{1}{2}\int_\Omega\mathbf{v}^t(\nabla\mathbf{u}_0+\nabla\mathbf{u}_0^t)\mathbf{v}\,d\mathbf{x}}{\frac{1}{2}\int_\Omega|\mathcal{D}(\mathbf{v})|^2\,d\mathbf{x}+\oint_\Gamma(\beta/\nu)\,|P_T\mathbf{v}|^2\,ds}.\end{aligned} \tag{40}$$

Thus for potential flow

$$\nu\,\lambda_{\nu,\beta}=\lambda_{1,-2}. \tag{41}$$

A similar remark follows for all eigenvalues since they are critical points of the Rayleigh quotient in (40). Alternatively, we can see that the scaling is valid for the PDE system (24), not only for the Rayleigh quotient. This gives us the option to compute all eigenvalues for potential flow with $\nu=1$ and $\beta=-2$, and then simply divide by ν.

In general, the bound (38) shows that

$$\nu\,|\lambda_{\nu,\beta}|\le C_{\beta/\nu}\sup_{\mathbf{x}\in\Omega}\|\nabla\mathbf{u}_{\nu,\beta}(\mathbf{x})\|_F. \tag{42}$$

Thus for general ν and β, we have an approximate scaling rule (42) instead of the exact scaling rule (41) for potential flow. We will show by numerical computations in Table 3 that the rule

$$\nu\,\lambda_{\nu,\beta}\approx\ \text{constant} \tag{43}$$

holds to a remarkable extent.

The instability condition in Theorem 2.2 is that $\lambda_{\nu,\beta}<-1$. For potential flow, with $\beta/\nu=-2$, we have instability when

$$\nu<-\lambda_{1,-2}.$$

3.4. Rate of Growth of Instability

From (19), we know that

$$\frac{\frac{1}{2}\frac{d}{dt}\int_\Omega |\mathbf{v}|^2\,d\mathbf{x}}{\frac{1}{2}\nu\int_\Omega |\mathcal{D}(\mathbf{v})|^2\,d\mathbf{x}+\oint_\Gamma \beta\,|P_T\mathbf{v}|^2\,ds} = -1-\frac{\frac{1}{2}\int_\Omega \mathbf{v}^t(\nabla\mathbf{u}_0+\nabla\mathbf{u}_0^t)\mathbf{v}\,d\mathbf{x}}{\frac{1}{2}\nu\int_\Omega |\nabla\mathbf{v}|^2\,d\mathbf{x}+\oint_\Gamma \beta\,|P_T\mathbf{v}|^2\,ds} = -1-\lambda \tag{44}$$

at $t=0$ if $\mathbf{v}(t=0)$ is the most unstable mode with eigenvalue λ. Here we are dropping the dependence on ν and β for the moment. Therefore

$$\frac{d}{dt}\int_\Omega |\mathbf{v}|^2\,d\mathbf{x} = (-1-\lambda)\left(\frac{\nu}{2}\int_\Omega |\nabla\mathbf{v}|^2\,d\mathbf{x}+\oint_\Gamma \beta\,|P_T\mathbf{v}|^2\,ds\right). \tag{45}$$

If $\lambda<-1$, then the kinetic energy of the perturbation grows with a positive rate

$$r=-1-\lambda. \tag{46}$$

In particular, this completes the proof of Theorem 2.1.

We can relate (45) to a more familiar expression for energy growth as follows. First, define the kinetic energy $k(t)=\int_\Omega |v(\mathbf{x},t)|^2\,d\mathbf{x}$. Second, divide (45) by $k(t)$ to get

$$\frac{d}{dt}\log k(t) = r\,\frac{\frac{1}{2}\nu\int_\Omega |\nabla\mathbf{v}|^2\,d\mathbf{x}+\oint_\Gamma \beta\,|P_T\mathbf{v}|^2\,ds}{\int_\Omega |\mathbf{v}|^2\,d\mathbf{x}} \geq \frac{r\nu}{C_{\beta/\nu}}, \tag{47}$$

where C_b is the constant in the Poincaré inequality (27), valid for all $\mathbf{v}\in V$ and for $b>-b_0$, where $b_0>0$ depends on the domain. The inequality (47) implies that kinetic energy k grows at least as fast as an exponential with exponent $r\nu/C_{\beta/\nu}$, at least initially. For sufficiently smooth data, this would hold in a neighborhood of zero, but in general holds only at $t=0$.

3.5. Spaces of Perturbations

Suppose that the eigenproblem (24) has several eigenvalues satisfying

$$\lambda_1\leq\lambda_2\leq\cdots\lambda_k<-1 \tag{48}$$

with corresponding eigenfunctions $\mathbf{v}_i$. Then any combination of the $\mathbf{v}_i$'s can lead to a growing perturbation, as follows.

Let us introduce some notation involving bilinear forms:

$$\begin{aligned} a(\mathbf{u},\mathbf{v}) &= \frac{\nu}{2}\int_\Omega \mathcal{D}(\mathbf{u}):\mathcal{D}(\mathbf{v})\,d\mathbf{x}+\oint_\Gamma \beta\,\mathbf{u}\cdot\mathbf{v}\,ds,\\ \mathcal{B}_{\mathbf{u}}(\mathbf{v},\mathbf{w}) &= \frac{1}{2}\int_\Omega \mathbf{v}^t(\nabla\mathbf{u}+\nabla\mathbf{u}^t)\mathbf{w}\,d\mathbf{x}. \end{aligned} \tag{49}$$

Then the eigenvalue problem may be written as

$$a(\mathbf{v}_i,\mathbf{w}) = \lambda_i^{-1}\mathcal{B}_{\mathbf{u}}(\mathbf{v}_i,\mathbf{w}) \quad \forall\mathbf{w}\in V, \tag{50}$$

where V is the subset of $H^1(\Omega)^d$ consisting of divergence-free functions vanishing on the boundary, defined in (4). As is well known, the eigenvectors can be chosen to be orthogonal in the sense that

$$a(\mathbf{v}_i,\mathbf{v}_j)=0=\mathcal{B}_{\mathbf{u}}(\mathbf{v}_i,\mathbf{v}_j) \quad \forall i\neq j.$$

Consider

$$\mathbf{v}=\sum_{i=1}^{k} c_j\mathbf{v}_j. \tag{51}$$

TABLE 1. *Values of the smallest eigenvalue λ for two-dimensional domains of size S. The definition of the domain size S is given in (54). The choice of β for these computations was $\beta = 0$*

S	8	12	16	32	64	128
λ	-0.123	-0.151	-0.178	-0.275	-0.429	-0.638

Then

$$\frac{-\mathcal{B}_{\mathbf{u}}(\mathbf{v},\mathbf{v})}{a(\mathbf{v},\mathbf{v})} = \frac{\sum_{i=1}^{k} c_j^2(-\lambda_i)a(\mathbf{v}_i,\mathbf{v}_i)}{\sum_{i=1}^{k} c_j^2 a(\mathbf{v}_i,\mathbf{v}_i)} \geq -\lambda_k. \tag{52}$$

Thus

$$a(\mathbf{v},\mathbf{v}) \leq \lambda_k^{-1}\mathcal{B}_{\mathbf{u}}(\mathbf{v},\mathbf{v}),$$

and the conditions for energy instability at the beginning of Sect. 2.3 are satisfied if $\lambda_k < -1$. In this case, the entire span of $\mathbf{v}_1, \ldots, \mathbf{v}_k$ can lead to instability. Summarizing these arguments, we have proved the following.

Theorem 3.1. *Consider the eigenvalues specified in (48). If $\lambda_k < -1$, the flow $\mathbf{u}$ is energy unstable at $t = 0$, with any initial perturbation $\mathbf{v}$ of the form (51) being an unstable mode.*

The most negative eigenvalues correspond potentially to the most unstable modes, and by contrast the most positive eigenvalues correspond to the most stable modes. For this reason, we consider both extremes computationally.

4. Example: Flow Around a Cylinder

Flow around a cylinder is one of the most widely studied phenomena in fluid mechanics, from theoretical, experimental, and computational points of view. In sect. 5, we examine stable and unstable perturbations of this flow. With this in mind, we first give some background on this topic.

The Reynolds number is $R = UL/\hat{\nu}$, where $\hat{\nu}$ is the kinematic viscosity and typical choices are $U =$ the free-stream speed and $L =$ the diameter of the cylinder. To see what Reynolds numbers are of practical interest, consider the following. For air at -40 degrees (F or C), $\hat{\nu} = 0.1$ cm^2/sec. Thus $R = 10^3$ for $L = 1$ centimeter and $U = 1$ meter per second ($= 3.6$ kilometers per hour, a leisurely walking speed). In our computations, we took the radius of the cylinder to be 1, so $L = 2$. Similarly, the free-stream speed $U \approx 1$, so $R \approx 2/\hat{\nu}$.

The flow around a cylinder is quite complex but well studied at low Reynolds numbers. The flow is steady until about $R = 50$ when the the Karman vortex street (Hopf bifurcation) occurs. This corresponds to $\nu \approx 0.04$ in our computations. Near $R = 200$, three-dimensional vortices appear, with various modes (A,B,A*) [18] and hysteresis. Not much is reported beyond that until the drag crisis [16,24], at about $R = 5 \times 10^5$.

4.1. Domain Size Dependence

The base flows (for positive Reynolds numbers) around a cylinder are known [9,10] to decay sufficiently fast at infinity that they can be approximated effectively on a finite box, as indicated in Fig. 2. But the eigenproblems behave differently, since there is no advection term. Solutions of the Stokes equations for flow around a cylinder [9,11] do not decay at infinity. They are in the space $H^1_w(\Omega)$ defined by the norm [11]

$$\|\mathbf{v}\|_{H^1_w(\Omega)} = \sqrt{\int_\Omega |\nabla \mathbf{v}(\mathbf{x})|^2 + \left(1 + |\mathbf{x}| \log |\mathbf{x}|\right)^{-2} |\mathbf{v}(\mathbf{x})|^2 \, d\mathbf{x}}. \tag{53}$$

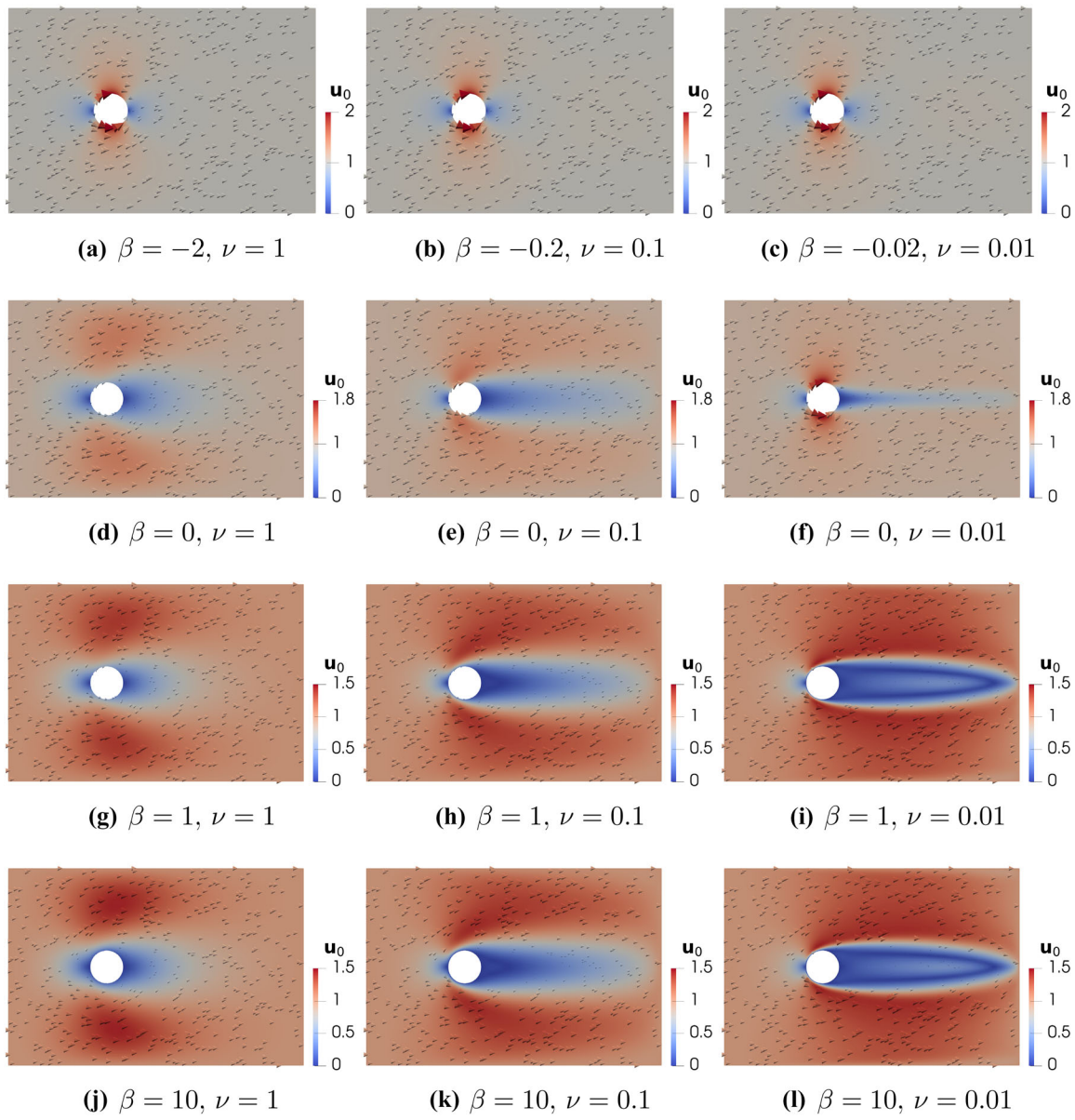

FIG. 2. Base flows for the indicated values of ν and β. The top row, with $\beta = -2\nu$, corresponds to potential flow. The computations were done in a box of dimensions 18×12, and the cylinder of radius 1 is centered in the box vertically and one third of the way from inlet to outlet. This is the domain S_{12} as defined in (54). Dirichlet/Stokes conditions on the boundary of the box were given by the potential flow solution

A Poincaré inequality holds for this space, but to use it to replace (36) would require the gradient of the base flow to decay sufficiently fast. However, the best estimates [10, Remark XII.8.3] for the decay rate suggests this is not valid. Thus we expect the eigenvalues for the two-dimensional problem to increase as the size of the domain increases. We have verified this in Table 1, where the parameter S is defined as follows. Define the computational domain Ω_S to be

$$\Omega_S = \left\{ \mathbf{x} \in \mathbb{R}^2 \ : \ -S/2 < x_1 < S, \quad |x_2| < S/2 \right\}. \tag{54}$$

Thus the domain used in Fig. 1 is for $S = 4$, whereas the subsequent figs. 2, 3, 7, and 8 and tables 2 and 3(a–d) are for $S = 12$.

Therefore, we have chosen to present our eigencomputations on a fixed domain. The data presented here are for small domains, to maximize the quality of the images. However, we have an on-line database of computations for various domain sizes at Zenodo[1].

Thus the eigenproblem for an infinite cylinder involves infinite eigenvalues, so the relationship between the 2D and 3D cases is only formal. However, we will see that the 2D computations for a bounded domain give valuable guidance regarding the 3D case. In particular, the on-line database shows that the form of the 2D eigenfunctions does not change as the domain size S is increased. They just spread out a bit.

4.2. Base Flows

The details regarding numerical implementation of (6) are given in appendix A.5.

In Fig. 1(a), we show the solution of the Navier-Stokes equations (1,2,3) with $\nu = 1$ and $\beta = -2$. This turns out to be the same as potential flow, described in sect. 4.3. By contrast, we show in Fig. 1(b) the solution of the Navier-Stokes equations (1,2,3) for $\nu = 1$ with $\beta = 2$. We see that the tangential flow has been substantially retarded by the Navier boundary condition (3). Details regarding the computations are given in the caption to Fig. 1.

Figure 2 explores other values of β and ν. In Fig. 2, the computations were done in a box of dimensions 18×12, and the cylinder of radius 1 is centered vertically and placed one-third of the way from the inflow (left) side of the box. Dirichlet/Stokes conditions on the boundary of the box were given by the potential flow solution. Table 2 also indicates the dependence of flow around a cylinder on ν and β.

In the 3D case, the size of the domain in the direction parallel to the cylinder was 12, and the (Dirichlet) boundary conditions on the ends of the box were given by the 2D base flow.

4.3. Potential Flow

Potential flow provides an exact solution of the Navier-Stokes equations that is independent of Reynolds number, as we review in sect. A.3. The potential equation is well posed with pure slip boundary conditions, but obtaining this as a solution of the Navier–Stokes equations requires appropriate Navier friction boundary conditions. In particular, Table 2 shows that you do not get the potential flow solution by taking $\beta = 0$.

Potential flow around a cylinder of radius 1 and aligned with the z-axis is given by $\mathbf{u} = \nabla\phi$ where p is given in (57):

$$\phi(x, y, z) = x + \frac{x}{x^2 + y^2}.$$

We can take the normal and tangent vectors on the cylinder to be

$$\mathbf{n} = -(x, y, 0), \qquad \boldsymbol{\tau}_1 = (y, -x, 0), \qquad \boldsymbol{\tau}_2 = (0, 0, 1).$$

The potential flow solution satisfies $\mathbf{u} \cdot \boldsymbol{\tau}_2 \equiv 0$ and by direct calculation (sect. A.4), we find that $\mathbf{n}^t(\nabla\mathbf{u})\boldsymbol{\tau}_2 = 0$ and

$$\mathbf{n}^t(\nabla\mathbf{u})\boldsymbol{\tau}_1 = 2y = \mathbf{u} \cdot \boldsymbol{\tau}_1$$

on the cylinder. Thus (3) is satisfied for $\beta = -2\nu$.

In sect. A.2, an explicit formula for $\nabla\mathbf{u}$ for potential flow suggests some possible features of unstable modes.

[1] https://zenodo.org/record/6566937#.YoeotDlBxMk.

TABLE 2. *Difference* $\|\mathbf{u}_0 - \mathbf{u}_{pf}\|_{H^1}$. $\mathbf{u}_0$ *is the solution of the Navier–Stokes equations for a given* ν *and* β, *and* $\mathbf{u}_{pf}$ *is the solution of the Navier–Stokes equations for* $\beta = -2\nu$, *that is, potential flow. The computational domain was chosen to be* S_{12}, *cf. (54)*

β	ν		
	1	0.1	0.01
0	2.19	2.19	0.94
10	3.02	3.93	5.48
100	3.24	3.97	5.48

4.4. Dependence on β

Table 2 indicates how the solution differs from potential flow as a function of ν and β. We see substantial dependence on ν, as expected, but little dependence on β for β sufficiently large. Here $\mathbf{u}_0$ denotes the base flow, depending on ν and β, for which we will measure the basic instabilities. And $\mathbf{u}_{pf}$ denotes potential flow, the solution for $\beta = -2\nu$ for all ν. Figure 2 depicts these flows.

4.5. General Geometries

As noted following (3), it makes sense to have separate friction coefficients β_k for the different tangential directions, and that they can vary as functions of space. Thus (68) gives a general prescription for choosing β to make the solution of the Navier–Stokes equations with Navier slip/friction boundary conditions the same as potential flow, for any geometry:

$$\beta_k = -\frac{\nu\,\mathbf{n}^t(\nabla\mathbf{u} + \nabla\mathbf{u}^t)\boldsymbol{\tau}_k}{\mathbf{u}\cdot\boldsymbol{\tau}_k} = -\frac{2\nu\,\mathbf{n}^t(\nabla^2\phi)\boldsymbol{\tau}_k}{\nabla\phi\cdot\boldsymbol{\tau}_k}, \quad k = 1, 2. \tag{55}$$

For any flow $\mathbf{u}$, we can refer to the quotients β_k as the *effective Navier friction* for that flow. Thus the effective Navier friction for potential flow is equal to -2ν, and hence tends to zero with ν. Thus we can think of the effective friction as zero for the Euler equations.

5. Eigensolutions for the Cylinder

Here we explain the main conclusions regarding the unstable modes for flow around the cylinder. The main things to notice are two-fold. First, the instability eigenfunction is largely supported downstream of the cylinder. Second, an instability occurs at a lower Reynolds number than the one associated with the Karman vortex street. In addition, we add the following observations.

5.1. Eigenfunction Form

The form of the eigenfunctions shows very little variation as ν and β are varied. This is illustrated in Fig. 3 for the most unstable mode. We found this behavior to be pervasive for all modes and for every variation of β and ν (further data not shown). Curious readers are invited to download a dataset containing all the computed eigenmodes.

As seen in Fig. 3, the most unstable mode takes the form of two rotations aft of the cylinder. As ν decreases, the support of the eigenfunction moves downstream a bit from the cylinder. Figure 7 shows the two most unstable modes for $\nu = 0.1$ and $\beta = 10$, and Fig. 8 shows four the most unstable modes for $\nu = 0.01$ and $\beta = 10$. We see that the most unstable modes are all rotations, but that the frequency of the eigenmodes increases together with the associated eigenvalue.

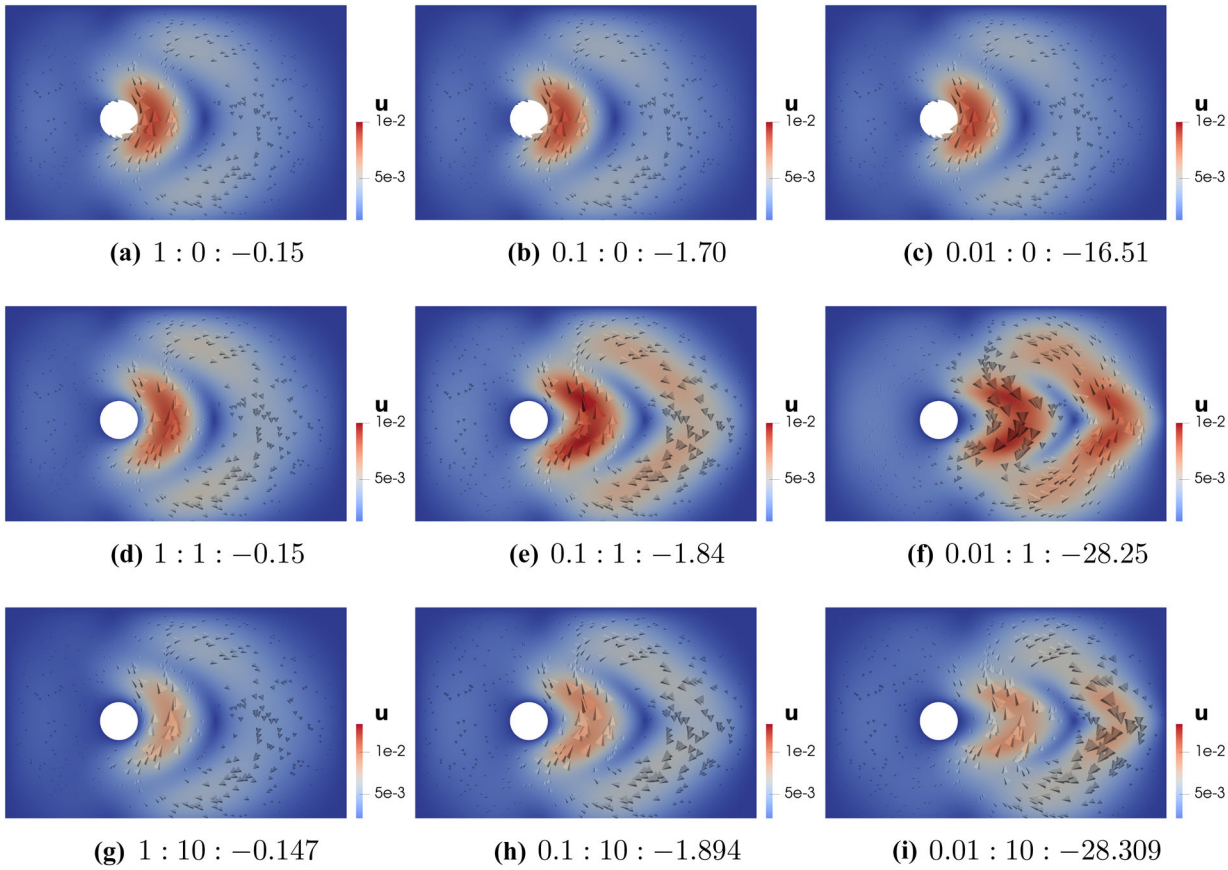

FIG. 3. Most unstable modes for values for flow past an infinitely long cylinder. Under each figure is listed the triple of values $\nu : \beta : \lambda$. The perturbations are identified by computing the eigenmode $\mathbf{v}$ with the most negative associated eigenvalue λ. Flow modes are shown for values of $\nu \in \{0.01, 0.1, 1.0\}$ and $\beta \in \{0, 1, 10\}$. The most unstable mode was consistently identified as a downstream rotation. Note that the eigenmodes are invariant with respect to multiplication by a scalar. In particular, $\mathbf{v}$ and $-\mathbf{v}$ are equivalent, and thus the rotation direction is arbitrary, as seen in some panels. See the caption for Fig. 2 for more computational details

5.2. Eigenvalue Scaling Examined

The scaling 'law' indicated in (43), and anticipated in the inequality (42), is largely supported in Table 3, albeit only approximately. Thus the eigenvalues grow like ν^{-1} as ν is decreased. This occurs despite the fact that the wake region of the base flow is increasing.

5.3. Another Scaling Relation

We know from the scaling law (43) that the quantity β/ν influences the relationship between viscous energy and the boundary integral in the variational formulation (24). Thus it is not surprising that we obtain more and more digits of agreement for the eigenvalues for fixed values of β as ν is reduced (compare subtables (c) and (d), or subtables (g) and (h), in Table 3). Even though β is fixed, the quantity β/ν is increasing by a factor of ten each time ν is reduced by a factor of ten. Each time ν is reduced by a factor of ten, the agreement between eigenvalues increases by one digit (i.e., a factor of ten), as we go from $\nu = 1$ to $\nu = 0.001$. This leads to the following conjecture. Number the eigenvalues $\lambda_1 < \lambda_2 < \cdots$.

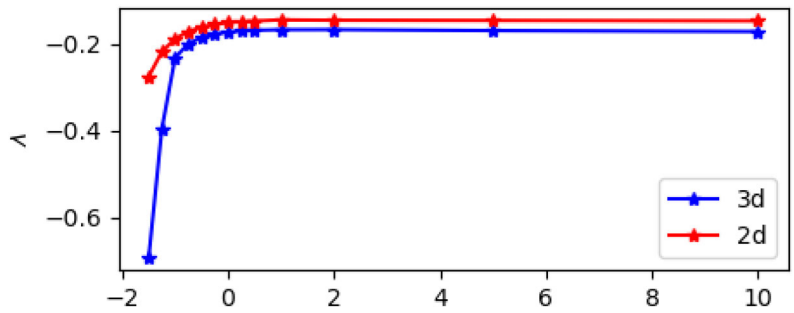

FIG. 4. Minimum eigenvalue with $\nu = 1$, $\gamma = 25$ and varying β. The computational domain for 2D was Ω_{12} as defined in (54). For 3D, the domain was $\Omega_{12} \times [0, 20]$

Then the data in Table 3 suggest that

$$|\lambda_n^{\nu,\beta} - \lambda_n^{\nu,\infty}| \leq C\lambda_n^{\nu,\infty}\frac{\nu}{\beta}, \tag{56}$$

where λ_n^{∞} is the apparent limit. Thus the typical issues that one would worry about (small ν and large β) become irrelevant in terms of instabilities. This is consistent with the observation that the unstable modes all are quite small on the boundary of the cylinder, so it is reasonable to conjecture that they tend to zero there as $\nu/\beta \to 0$.

5.4. Most Unstable Mode and β Scaling

Figure 4 presents the lowest eigenvalue as a function of β for $\nu = 1$. Not surprisingly, the 3D lowest mode has a smaller eigenvalue than the 2D case, since the 3D mode is the result of minimizing over a much larger space. For $\beta \leq 0$ the flow becomes significantly more unstable as β decreases. Physically this can be interpreted as the instabilities growing as the flow is being accelerated more and more over the cylinder boundary.

Figure 5 shows how the flow field changes as β is increased from $\beta = -2$ (corresponding to potential flow) to $\beta = -1$. For potential flow the most unstable mode is a single rotation around the cylinder. As β increases the instability mode develops a second rotation aft of the cylinder. In Fig. 3 we see that for $\beta \geq 0$ the instability eigenvalue does not change significantly with respect to β. This is consistent with Fig. 4.

5.5. 2D Versus 3D Modes

All 2D modes are also 3D modes, but not conversely. Comparing panels (c) and (g), or panels (d) and (h), in Table 3 shows the interleaving of the 2D and 3D unstable modes.

As the number of periods in the z-direction increases for a given type of (2D) mode, the corresponding value of λ decreases (data not shown), as would be expected from examining the quotient (23), or its equivalent (52). As there are more oscillations in the z-direction, the $a(\cdot,\cdot)$ form increases, since it involves derivatives in the z-direction, whereas the $\mathcal{B}$ form does not.

6. Conclusions

We used the theory of kinetic-energy instability [33,34] to exhibit instabilities of steady flow past a cylinder subject to slip boundary conditions with friction. One such solution is given by potential flow with a negative friction coefficient.

TABLE 3. Numerical evidence of a scaling law. Eigenvalues λ_n in $2d$ (left) and $3d$ (right) computed for different values of β and ν. The scaling law holds exactly when $\beta = -2$. This scaling gets less evident as β increases. See the caption for Fig. 2 for more computational details. The computational domain for 2D was Ω_{12} as defined in (54). For 3D, the domain was $\Omega_{12} \times [0, 20]$

$d=2$					$d=3$				
n	ν				n	ν			
	1	0.1	0.01	0.001		1	0.1	0.01	0.001
(a) λ_n for $\beta = -2\nu$					(e) λ_n for $\beta = -2\nu$				
1	−1.113	−11.126	−111.243	−1111.937	1	−0.968	−9.659	−96.359	−958.334
2	−0.082	−0.813	−8.106	−81.024	2	−0.642	−6.408	−63.896	−636.055
3	−0.068	−0.683	−6.806	−67.994	3	−0.403	−4.026	−40.223	−401.268
4	−0.045	−0.444	−4.441	−44.389	4	−0.367	−3.663	−36.606	−365.206
5	−0.038	−0.378	−3.784	−37.829	5	−0.242	−2.414	−24.135	−240.875
6	−0.033	−0.327	−3.276	−32.142	6	−0.233	−2.326	−23.257	−232.088
(b) λ_n for $\beta = 0$					(f) λ_n for $\beta = 0$				
1	−0.151	−1.698	−16.508	−149.612	1	−0.173	−1.886	−18.300	−180.305
2	−0.091	−1.091	−8.575	−61.466	2	−0.156	−1.744	−17.605	−165.344
3	−0.051	−0.716	−5.548	−39.358	3	−0.130	−1.474	−14.980	−141.330
4	−0.048	−0.602	−5.129	−34.3172	4	−0.106	−1.237	−13.937	−136.989
5	−0.040	−0.508	−4.152	−32.038	5	−0.096	−1.171	−12.012	−120.061
6	−0.039	−0.401	−3.777	−29.880	6	−0.091	−1.087	−10.450	−107.758
(c) λ_n for $\beta = 1$					(g) λ_n for $\beta = 1$				
1	−0.146	−1.838	−28.249	−398.780	1	−0.167	−2.126	−34.651	−497.382
2	−0.092	−1.400	−24.797	−343.552	2	−0.151	−1.898	−30.424	−433.588
3	−0.052	−0.860	−15.301	−210.024	3	−0.126	−1.645	−27.158	−381.081
4	−0.048	−0.643	−12.883	−183.994	4	−0.101	−1.471	−25.940	−362.281
5	−0.042	−0.626	−10.226	−140.031	5	−0.096	−1.305	−22.568	−311.305
6	−0.041	−0.550	−9.442	−138.351	6	−0.090	−1.261	−20.977	−291.879
(d) λ_n for $\beta = 10$					(h) λ_n for $\beta = 10$				
1	−0.147	−1.894	−28.309	−398.856	1	−0.172	−2.213	−34.791	−497.562
2	−0.097	−1.453	−24.846	−342.610	2	−0.153	−1.961	−30.530	−433.723
3	−0.053	−0.887	−15.327	−210.045	3	−0.128	−1.709	−27.231	−381.175
4	−0.051	−0.664	−12.911	−184.007	4	−0.102	−1.533	−26.033	−362.391
5	−0.046	−0.661	−10.324	−140.083	5	−0.099	−1.351	−22.619	−311.363
6	−0.045	−0.585	−9.474	−138.414	6	−0.093	−1.295	−21.040	−291.953

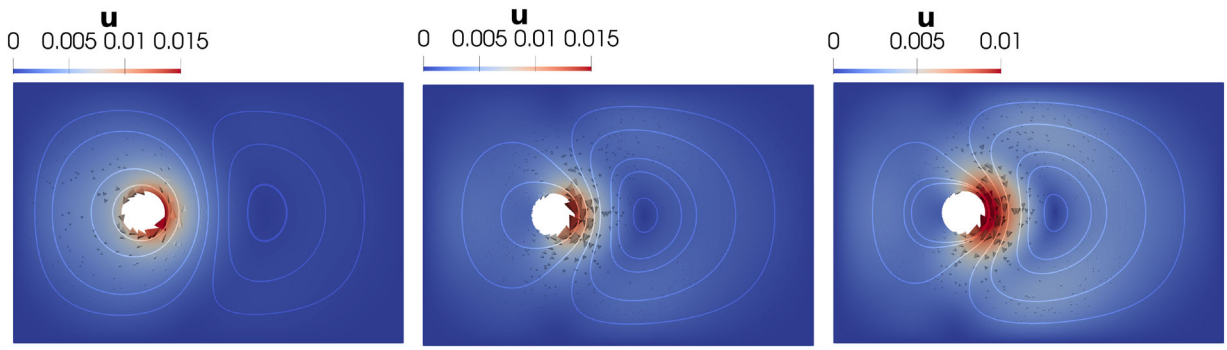

(a) $\beta = -2$ **(b)** $\beta = -1.5$ **(c)** $\beta = -1$

FIG. 5. Most unstable modes in 2D for $\nu = 1$ and $\beta \in \{-2, -1.5, -1\}$. For $\beta = -2$ the eigenmode is a single rotation around the cylinder. As the friction increases the eigenmode develops a second rotation aft of the cylinder

We computed numerically the eigenproblem determining the most unstable modes. These correspond to modes previously observed in dynamic simulations [17]. The most striking observation is that the most unstable modes are supported primarily downstream of the cylinder, typically well separated from the back of the cylinder.

The kinetic-energy instability theory was developed here for general bluff-body flows, and the computational techniques developed in [12] and applied here could be used for general geometries [17], including complete aircraft.

Acknowledgements. We thank Miroslav Kuchta for assistance.

Declarations

Competing Interests The author(s) declares that they have no competing interests.

Publisher's Note Springer Nature remains neutral with regard to jurisdictional claims in published maps and institutional affiliations.

A. Additional figures and information

Here we collect additional information regarding potential flow and the computational techniques used.

A.1. Potential Flow Details

Potential flow around a cylinder of radius 1 and aligned with the z-axis is given by $\mathbf{u} = \nabla\phi$ where

$$\phi(x, y, z) = \phi(r, \theta, z) = \left(ar + \frac{1}{r}\right)\cos\theta = ax + \frac{x}{x^2 + y^2}, \tag{57}$$

where the constant a must be adjusted to incorporate the boundary conditions on the cylinder. If $a = 1$, it satisfies the pure slip boundary condition $\mathbf{u} \cdot \mathbf{n} = 0$ on the cylinder. Otherwise, we have

$$\nabla\phi \cdot \mathbf{n} = (a - 1)\cos\theta = \frac{a - 1}{a + 1}\phi$$

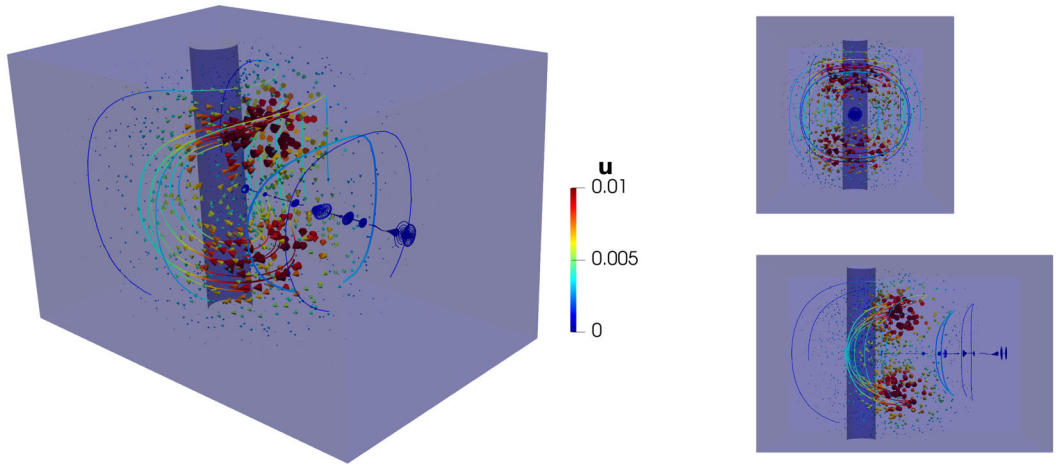

(a) Eigenmode corresponding to smallest eigenvalue $\lambda = -0.172$

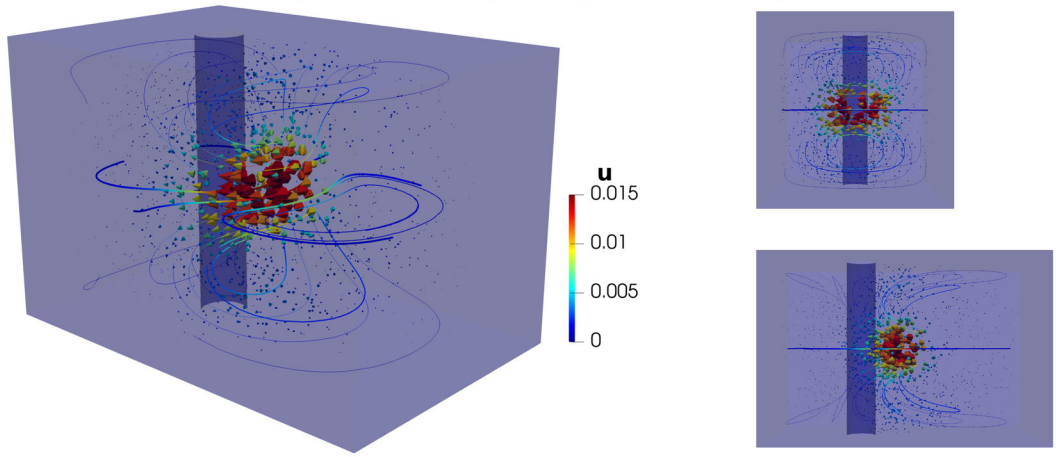

(b) Eigenmode corresponding to second smallest eigenvalue $\lambda = -0.153$

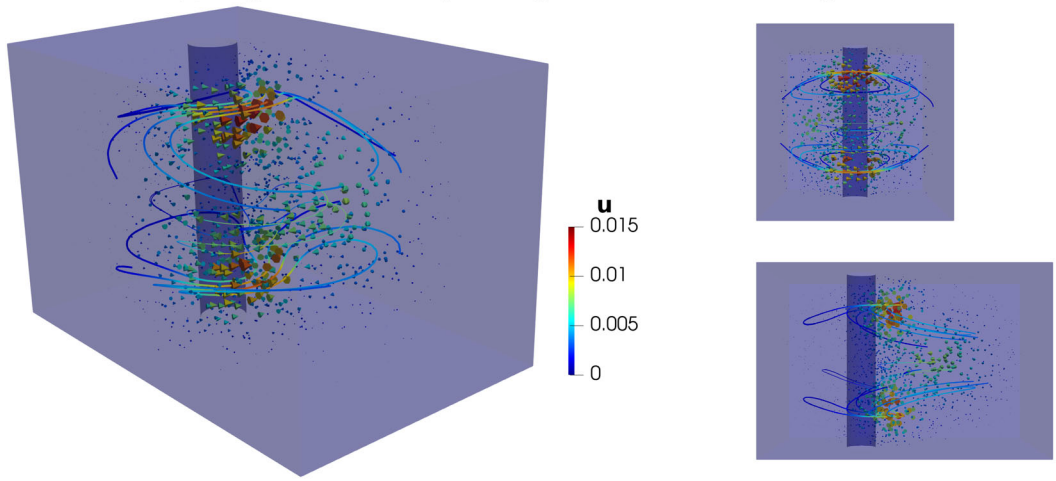

(c) Eigenmode corresponding to third smallest eigenvalue $\lambda = -0.128$

FIG. 6. Three-dimensional most unstable modes for $\nu = 1$ and $\beta = 10$, seen in profile (left), from the front (top right) and from the side (bottom right). The extreme modes for 3D are similar to the extreme modes for 2D, but with modal behavior in the z-direction. The size of the domain here was $18 \times 12 \times 20$, that is, $\Omega_{12} \times [0, 12]$, cf. (54)

on the cylinder. The velocity components are given by

$$u_x(x,y,z) = a - \frac{x^2-y^2}{\left(x^2+y^2\right)^2}, \qquad u_y(x,y,z) = \frac{-2xy}{\left(x^2+y^2\right)^2}, \qquad u_z = 0. \tag{58}$$

Thus $|\mathbf{u}(\mathbf{x})| \to a$ as $\mathbf{x} \to \infty$. On the cylinder $(x^2+y^2=1)$, with $a=1$,

$$\mathbf{u}(x,y) = (2y^2, -2xy, 0)^t, \qquad |\mathbf{u}| = 2|y|. \tag{59}$$

In particular, the flow speed does not depend on x. From now on, we take $a=1$.

We can take the characteristic length L to be the radius of the cylinder, that is, $L=1$. We can take the characteristic velocity U to be 1 (the speed at infinity if $a=1$). Thus the Reynolds number $R = UL/\nu$ is simply $R = 1/\nu$.

By simple calculus, we can compute $\nabla\mathbf{u}$:

$$r^6\,\nabla\mathbf{u} = \left(x^2+y^2\right)^3 \nabla\mathbf{u} = \begin{pmatrix} 2x^3-6xy^2 & -2y^3+6x^2y & 0 \\ -2y^3+6x^2y & -2x^3+6xy^2 & 0 \\ 0 & 0 & 0 \end{pmatrix}. \tag{60}$$

Note that the constant a disappears from the expression for $\nabla\mathbf{u}$.

A.2. Examining ∇u: Rotational Modes

Analyzing the explicit formula (60) for $\nabla\mathbf{u}$ for potential flow can suggest the form of unstable modes. For all x and z, we have

$$\nabla\mathbf{u}(x,0,z) = \frac{1}{x^3}\begin{pmatrix} 2 & 0 & 0 \\ 0 & -2 & 0 \\ 0 & 0 & 0 \end{pmatrix}. \tag{61}$$

Note that

$$\nabla\mathbf{u}(x,0,z)\begin{pmatrix} 0 \\ 1 \\ \zeta \end{pmatrix} = -\frac{2}{x^3}\begin{pmatrix} 0 \\ 1 \\ 0 \end{pmatrix}, \tag{62}$$

for any $\zeta \in \mathbb{R}$. Therefore

$$\begin{pmatrix} 0 \\ \psi_z(x,y,z) \\ -\psi_y(x,y,z) \end{pmatrix}^t \nabla\mathbf{u}(x,0,z) \begin{pmatrix} 0 \\ \psi_z(x,y,z) \\ -\psi_y(x,y,z) \end{pmatrix} = -\frac{2}{x^3}\psi_z(x,y,z)^2, \tag{63}$$

for any function ψ, indicating instability of the perturbation

$$\mathbf{v} = (0, \psi_z, -\psi_y) \tag{64}$$

for $x > 0$, but stability for $x < 0$. Functions of the form (64) are divergence free. This heuristic calculation is consistent with the observation [17] of vortices rotating in the y,z plane, indicated in Figures 11 and 13 in [17] for flow past a cylinder. It also suggests that taking ψ constant in z would not lead to an instability, since (63) is zero if $\psi_z = 0$.

Since the perturbation (64) is stable at the front of the cylinder, we consider a different perturbation. For perturbations in the $x-z$ plane, of the form

$$\mathbf{v} = (\psi_z, 0, -\psi_x),$$

rotating around the y-axis, the expression analogous to (63) is negative. But the no-penetration condition $\mathbf{v}\cdot\mathbf{n} = 0$ on the front of the cylinder implies that $\psi_z = 0$ there, and thus does not lead to a substantial instability contribution. Therefore we expect the most unstable mode to have a small magnitude at the leading edge of the cylinder.

Perturbations of the form $\mathbf{v} = (\psi_y, -\psi_x, 0)$ correspond to two-dimensional modes. Then (62) again implies

$$\begin{pmatrix} \psi_y(x,y,z) \\ -\psi_x(x,y,z) \\ 0 \end{pmatrix}^t \nabla\mathbf{u}(x,0,z) \begin{pmatrix} \psi_y(x,y,z) \\ -\psi_x(x,y,z) \\ 0 \end{pmatrix} = -\frac{2}{x^3}\left(\psi_x(x,y,z)^2 + \psi_x(x,y,z)^2\right) \tag{65}$$

for any function ψ, indicating instability of the perturbation as long as it is concentrated near the centerline $y = 0$ and for $x > 0$.

A.3. Verifying the Equations

The verification that potential flow is a solution of Navier-Stokes stems from the vector-calculus identity

$$\mathbf{u}\cdot\nabla\mathbf{u} + \mathbf{u}\times(\nabla\times\mathbf{u}) = \tfrac{1}{2}\nabla|\mathbf{u}|^2. \tag{66}$$

For $\mathbf{u} = \nabla\phi$, $\nabla\times\mathbf{u} = \mathbf{0}$. Since $\Delta\phi = 0$, $\Delta\mathbf{u} = \nabla\Delta\phi = \mathbf{0}$. Thus with $\mathbf{u} = \nabla\phi$,

$$-\nu\Delta\mathbf{u} + \mathbf{u}\cdot\nabla\mathbf{u} = \frac{1}{2}\nabla|\mathbf{u}|^2,$$

and we have a solution of (1) for any ν with

$$p = -\frac{1}{2}|\mathbf{u}|^2 = -\frac{1}{2}|\nabla\phi|^2. \tag{67}$$

Thus the expression in (57) with $a = 1$ gives a steady solution of Navier-Stokes with p as given in (67).

The natural form of dissipation in Navier-Stokes is $\nabla\cdot\left(\nabla\mathbf{u} + \nabla\mathbf{u}^t\right)$. But

$$\nabla\cdot\left(\nabla\mathbf{u} + \nabla\mathbf{u}^t\right) = \Delta\mathbf{u} + \nabla(\nabla\cdot\mathbf{u}),$$

so the two forms are equivalent for divergence-free functions.

A.4. Potential Flow Boundary Conditions

The boundary condition (3) is satisfied if the friction coefficient β satisfies

$$\beta\,\mathbf{u}\cdot\boldsymbol{\tau}_k = -\nu\,\mathbf{n}^t(\nabla\mathbf{u} + \nabla\mathbf{u}^t)\boldsymbol{\tau}_k, \quad k = 1, 2. \tag{68}$$

We can take the normal and tangent vectors on the cylinder to be

$$\mathbf{n} = -(x, y, 0), \qquad \boldsymbol{\tau}_1 = (y, -x, 0), \qquad \boldsymbol{\tau}_2 = (0, 0, 1).$$

Since the potential flow solution satisfies $\mathbf{u}\cdot\boldsymbol{\tau}_2 \equiv 0$ and

$$(\nabla\mathbf{u})^t\boldsymbol{\tau}_2 = (\nabla\mathbf{u})\boldsymbol{\tau}_2 = \left(x^2+y^2\right)^{-3} \begin{pmatrix} 2x^3 - 6xy^2 & -2y^3 + 6x^2y & 0 \\ -2y^3 + 6x^2y & -2x^3 + 6xy^2 & 0 \\ 0 & 0 & 0 \end{pmatrix} \begin{pmatrix} 0 \\ 0 \\ 1 \end{pmatrix} = \mathbf{0}, \tag{69}$$

the equation in (68) for $k = 2$ is satisfied for any β. From (59), we have

$$\mathbf{u}\cdot\boldsymbol{\tau}_1 = (2y^2, -2xy, 0)\cdot(y, -x, 0) = 2y^3 + 2x^2y = 2y \tag{70}$$

on the cylinder. Similarly, (60) implies

$$\begin{aligned}(\nabla \mathbf{u})\boldsymbol{\tau}_1 &= \begin{pmatrix} 2x^3-6xy^2 & -2y^3+6x^2y & 0 \\ -2y^3+6x^2y & -2x^3+6xy^2 & 0 \\ 0 & 0 & 0 \end{pmatrix} \begin{pmatrix} y \\ -x \\ 0 \end{pmatrix} \\ &= \begin{pmatrix} y(2x^3-6xy^2)-x(-2y^3+6x^2y) \\ y(-2y^3+6x^2y)-x(-2x^3+6xy^2) \\ 0 \end{pmatrix} \\ &= \begin{pmatrix} -4x^3y-4xy^3 \\ -2y^4+2x^4 \\ 0 \end{pmatrix} = \begin{pmatrix} -4xy \\ -2y^4+2x^4 \\ 0 \end{pmatrix}\end{aligned} \tag{71}$$

on the cylinder. Therefore

$$\mathbf{n}^t(\nabla \mathbf{u})\boldsymbol{\tau}_1 = -(x,y,0)\begin{pmatrix} -4xy \\ -2y^4+2x^4 \\ 0 \end{pmatrix} = 2y\big(2x^2+y^4-x^4\big). \tag{72}$$

But

$$2x^2+y^4-x^4 = 2x^2+(1-x^2)^2-x^4 = 1$$

on the cylinder. Thus the shear stress is equal to the tangential velocity, that is,

$$\mathbf{n}^t(\nabla \mathbf{u})\boldsymbol{\tau}_1 = 2y = \mathbf{u}\cdot\boldsymbol{\tau}_1 \tag{73}$$

on the cylinder. Therefore (68) is satisfied for $\beta = -2\nu$.

Thus potential flow for the cylinder provides an exact solution of Navier-Stokes for any Reynolds number, and without any boundary layer, for $\beta = -2$. This may be viewed as nonphysical, as it represents an active boundary condition: the tangential stress increases the tangential velocity. On the other hand, it may also be viewed as motivating concepts for active control of turbulence [5]. In any case, potential flow with $\beta = -2$ provides an exact solution for Navier-Stokes with Navier boundary conditions suitable for verifying an implementation, as we do in [12].

A.5. Numerical Implementation

The details regarding numerical implementation of (6) together with boundary conditions (2) and (3), are given in [12]. Briefly, we use lowest-order Taylor–Hood approximation with Nitsche's method [35,41] to enforce slip conditions in the limit of small mesh size.

We begin by approximating the domain with curved boundary by simplicial complexes Ω_h, where the edge lengths of Γ_h are of order h_Γ in size. Then conventional finite elements can be employed, with the various boundary expressions being approximated by appropriate quantities. In particular, we assume that Ω_h is triangulated with a non-degenerate mesh $\mathcal{T}_h$ of maximum simplex size h. We define the Taylor–Hood spaces

$$\begin{aligned} W_h^k &= \left\{\mathbf{v}\in C(\Omega_h)\ :\ \mathbf{v}=\mathbf{0} \text{ on } \Omega_h\backslash\Gamma_h,\ \mathbf{v}|_T\in\mathcal{P}_k(T)^d\ \forall\, T\in\mathcal{T}_h\right\}, \\ \Pi_h^k &= \left\{q\in L^2(\Omega_h)\ :\ q|_T\in\mathcal{P}_{k-1}(T)^d\ \forall\, T\in\mathcal{T}_h\right\}, \end{aligned}$$

and the Nitsche bilinear form

$$\begin{aligned} a_h((\mathbf{u},p,\rho),(\mathbf{v},q,\sigma)) &= \frac{\nu}{2}\int_{\Omega_h}\mathcal{D}(\mathbf{u}):\mathcal{D}(\mathbf{v})\,dx + \oint_{\Gamma_h}\sum_i \beta(\mathbf{u}\cdot\boldsymbol{\tau}_i)(\boldsymbol{\tau}_i\cdot\mathbf{v})\,ds \\ &+ \int_{\Omega_h}\rho\,q+\sigma\,p\,dx - \oint_{\Gamma_h}\mathbf{n}^t\big(\nu\mathcal{D}(\mathbf{u})-pI\big)\mathbf{n}(\mathbf{n}\cdot\mathbf{v})\,ds - \oint_{\Gamma_h}\mathbf{n}^t\big(\nu\mathcal{D}(\mathbf{v})-pI\big)\mathbf{n}(\mathbf{n}\cdot\mathbf{u})\,ds \\ &- (p,\nabla\cdot\mathbf{v})_h - (q,\nabla\cdot\mathbf{u})_h + \gamma h^{-1}\oint_{\Gamma_h}(\mathbf{u}\cdot\mathbf{n})(\mathbf{n}\cdot\mathbf{v})\,ds, \end{aligned} \tag{74}$$

where

$$(p,q)_h = \int_{\Omega_h} p\,q\,dx.$$

For normal and tangential vectors, we define the orthogonal projection π_h from Γ_h to Γ and we take $\mathbf{n}|_{\Gamma_h} = \mathbf{n}\circ\pi^h$ and $\boldsymbol{\tau}^i|_{\Gamma_h} = \boldsymbol{\tau}^i\circ\pi^h$, as analyzed in [12]. Then the Taylor–Hood approximation [32] finds $\mathbf{u}_h \in \mathbf{g}_I + W_h^k$, $p_h \in \Pi_h^k$, and $\rho\in\mathbb{R}$ satisfying

$$a_h((\mathbf{u}_h,p,\rho),(\mathbf{v},q,\sigma)) = \mathbf{f}(\mathbf{v}) \tag{75}$$

for all $(\mathbf{v},q,\sigma)\in W_h^k\times\Pi_h^k\times\mathbb{R}$, where $\mathbf{g}_I$ denotes a suitable interpolant of $\mathbf{g}$. This method satisfies

$$\|\mathbf{u}-\mathbf{u}_h\|_{H^1(\Omega)} \le C\big(h_\Gamma^{3/2}+h^k\big)$$

for $k\ge 2$ [12]. The approximation order cannot be higher than 3/2 due to the polygonal approximation of the boundary [2]. However, the results of [12] suggest substantial benefit if mesh refinement is done near Γ.

The nonlinear problem (6) involves solving (75) for $\mathbf{f}(\mathbf{v}) = -(\mathbf{u}\cdot\nabla\mathbf{u},\mathbf{v})$ via various techniques. Many automated systems will apply Newton's method automatically just based on the request to solve

$$a_h((\mathbf{u}_h,p,\rho),(\mathbf{v},q,\sigma)) + \int_{\Omega_h}(\mathbf{u}_h\cdot\nabla\mathbf{u}_h)\cdot\mathbf{v}\,dx = 0 \tag{76}$$

with the indicated spaces and Dirichlet boundary condition on $\partial\Omega\backslash\Gamma$. The cylinder problem, with potential function solution, has been used to validate the implementation of the algorithm (75) in [12].

For $\nu = 1$, we often used $\gamma = 25$. But we found that it was important to reduce γ as ν decreased. The general rule $\gamma = 100\,\nu$ worked well.

A.6. Eigenvalue Computation

The eigenvalue problem (24) requires solving the variational problem: find $(\mathbf{u}_h,p_h,\rho)\in W_h^k\times\Pi_h^k\times\mathbb{R}$ such that

$$a_h((\mathbf{u}_h,p,\rho),(\mathbf{v},q,\sigma)) = \lambda^{-1}\int_{\Omega_h}\mathbf{u}_h^t\big(\nabla\mathbf{u}+\nabla\mathbf{u}^t\big)\mathbf{v}\,dx \tag{77}$$

for all $(\mathbf{v},q,\sigma)\in W_h^k\times\Pi_h^k\times\mathbb{R}$. Since we use a mixed method to approximate the flow problem, the resulting matrix associated with the bilinear form $a_h(\cdot,\cdot)$ is of the form

$$\mathbf{A} = \begin{pmatrix} A_\beta & D & \mathbf{0}\\ D^t & \mathbf{0} & M\\ \mathbf{0} & M^t & 0\end{pmatrix}.$$

Suppose we pose the eigenproblem in the form

$$\mathbf{A}\begin{pmatrix}U\\P\\\rho\end{pmatrix} = \lambda^{-1}\begin{pmatrix}B&\mathbf{0}&\mathbf{0}\\\mathbf{0}&\mathbf{0}&\mathbf{0}\\\mathbf{0}&\mathbf{0}&0\end{pmatrix}\begin{pmatrix}U\\P\\\rho\end{pmatrix} = \lambda^{-1}\begin{pmatrix}BU\\\mathbf{0}\\0\end{pmatrix}, \tag{78}$$

where temporarily we use the notation U to denote the coefficients of $\mathbf{u}_h$ in W_h^k and similarly P to denote the coefficients of p_h in Π_h^k.

The last equation of the system (78) is $M^tP = 0$, which means that p_h has mean zero. Let us define

$$\overline{\Pi_h^k} = \Big\{q\in\Pi_h^k\ :\ \int_{\Omega_h} q\,dx = 0\Big\},$$

so that (78) implies that $p_h\in\overline{\Pi_h^k}$. The middle equation of the system (78) is $D^tU+\rho M = \mathbf{0}$, and so $\mathbf{u}_h$ is (weakly) divergence free. That is, $\mathbf{u}_h\in Z_h$ where

$$Z_h = \Big\{\mathbf{v}\in W_h^k\ :\ (q,\nabla\cdot\mathbf{v})_h = 0\ \forall q\in\overline{\Pi_h^k}\Big\}.$$

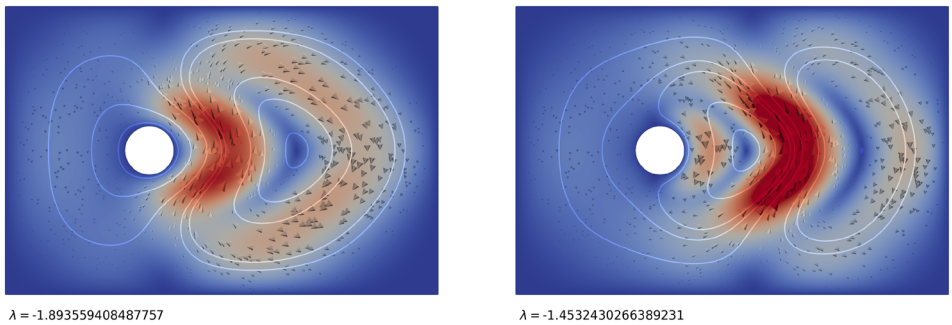

FIG. 7. Two most unstable modes in 2D for $\beta = 10$ and $\nu = 0.1$. See the caption for Fig. 2 for more computational details

The top equation of the system (78) is

$$A_\beta U + DP = \lambda^{-1} BU. \tag{79}$$

Consider the variational problem to find $\mathbf{u}_h \in Z_h$ such that

$$\begin{aligned} &\frac{\nu}{2}\int_{\Omega_h} \mathcal{D}(\mathbf{u}_h) : \mathcal{D}(\mathbf{v})\,dx + \oint_{\Gamma_h} \sum_i \beta(\mathbf{u}_h \cdot \boldsymbol{\tau}_i)(\boldsymbol{\tau}_i \cdot \mathbf{v})\,ds \\ &\quad - \oint_{\Gamma_h} \mathbf{n}^t\big(\nu\mathcal{D}(\mathbf{u}_h) - p_h I\big)\mathbf{n}(\mathbf{n}\cdot\mathbf{v})\,ds - \oint_{\Gamma_h} \mathbf{n}^t\big(\nu\mathcal{D}(\mathbf{v}) - p_h I\big)\mathbf{n}(\mathbf{n}\cdot\mathbf{u}_h)\,ds \\ &\quad + \gamma h^{-1}\oint_{\Gamma_h} (\mathbf{u}_h\cdot\mathbf{n})(\mathbf{n}\cdot\mathbf{v})\,ds = \lambda^{-1}\int_{\Omega_h} \mathbf{u}_h^t\big(\nabla\mathbf{u} + \nabla\mathbf{u}^t\big)\mathbf{v}\,dx \end{aligned} \tag{80}$$

for all $\mathbf{v} \in Z_h$. Expanding in basis functions, we see that (79) and (80) are equivalent. We recognize (80) as Nitsche's method applied to approximate (24).

A.7. Estimating C_b

The constant C_b in (29) can also be estimated by solving for $(\widetilde{\mathbf{v}}_h, p_h, \rho) \in W_h^k \times \Pi_h^k \times \mathbb{R}$ satisfying

$$a_h((\widetilde{\mathbf{v}}_h, p_h, \rho), (\mathbf{w}, q, \sigma)) = \lambda_b \int_{\Omega_h} \mathbf{w}^t \widetilde{\mathbf{v}}_h\,dx \tag{81}$$

for all $(\mathbf{w}, q, \sigma) \in W_h^k \times \Pi_h^k \times \mathbb{R}$. Then $C_b = 1/\lambda_b$. We can determine the limiting value b_0 in (35) by solving for $(\widetilde{\mathbf{v}}_h, p_h, \rho) \in W_h^k \times \Pi_h^k \times \mathbb{R}$ satisfying the eigenvalue problem

$$a_h((\widehat{\mathbf{v}}_h, p_h, \rho), (\mathbf{w}, q, \sigma)) = b_0 \oint_{\Gamma_h} \sum_i (\mathbf{w}\cdot\boldsymbol{\tau}_\pi^i)(\boldsymbol{\tau}_\pi^i \cdot \widehat{\mathbf{v}}_h)\,ds \tag{82}$$

for all $(\mathbf{w}, q, \sigma) \in W_h^k \times \Pi_h^k \times \mathbb{R}$.

A.8. Using SLEPc

We used the software system SLEPc [15] to compute eigenvalues for the system (78). We can rewrite (78) as

$$\mathbf{A}^{-1}\mathbf{B}X = \lambda X. \tag{83}$$

SLEPc writes this in terms of $\lambda^S = \lambda^{-1}$:

$$\mathbf{A}X = \lambda^S \mathbf{B}X.$$

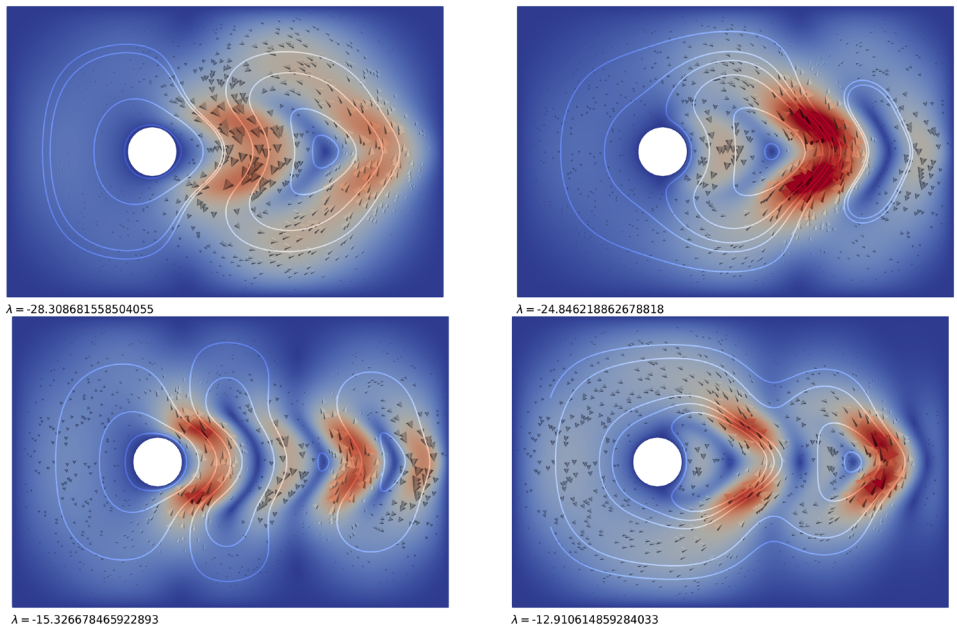

FIG. 8. Four most unstable modes in 2D for $\beta = 10$ and $\nu = 0.01$. See the caption for Fig. 2 for more computational details

Solving the eigenproblem for systems of this form is described in section 3.3.2 (Shift-and-invert) in the SLEPc manual [29]. In particular, [29, (3.7)] allows solving for

$$\big(\mathbf{A} - \sigma\mathbf{B}\big)^{-1}\mathbf{B}X = \theta X,$$

where σ is a user-defined shift. When $\sigma = 0$, we recover (83), and $\lambda = \theta$. When $\sigma \neq 0$, the eigenvalues θ, λ^S, and λ are related by

$$\lambda = \frac{\theta}{1 + \sigma\theta}, \qquad \theta = \frac{\lambda}{1 - \sigma\lambda} = \frac{1}{\lambda^S - \sigma}.$$

Note that the values of θ will be extreme when σ is close to $\lambda^{-1} = \lambda^S$. In view of (38), the eigenvalues λ that we seek lie in an interval $[-\Lambda, \Lambda]$. The mapping $\lambda \to \theta$ takes the λ interval $[-\Lambda, \Lambda]$ to the θ interval

$$\Big[\frac{-\Lambda}{1 + \sigma\Lambda}, \frac{\Lambda}{1 - \sigma\Lambda}\Big].$$

In this mapping, $\lambda = 0$ goes to $\theta = 0$ for any value of σ. Suppose $\sigma < 0$, and define $\rho = -\sigma\Lambda > 0$. Suppose further that $\rho < 1$. Then the interval $[-\Lambda, 0]$ is stretched out to $[-\Lambda/(1-\rho), 0]$ whereas $[0, \Lambda]$ is squeezed into $[0, \Lambda/(1+\rho)]$. In practice, we want to choose Λ large enough so that all of the λ's are contained in $[-\Lambda, \Lambda]$. Then we pick $\sigma = -\rho/\Lambda$ for $\rho < 1$. If by chance we pick $\sigma = -1/\Lambda$, then the λ interval $[-\Lambda, \Lambda]$ is mapped to the θ interval $[-\infty, \frac{1}{2}\Lambda]$.

If we know the value of the most negative λ, we pick σ such that

$$\lambda^{-1} < \sigma < 0.$$

But the closer σ is to λ^{-1}, the more separated the negative eigenvalues will be from the positive ones. As $\sigma \to 0$, the separation disappears.

References

[1] Bedrossian, Jacob, Germain, Pierre, Masmoudi, Nader: Stability of the Couette flow at high Reynolds numbers in two dimensions and three dimensions. Bull. Am. Math. Soc. **56**(3), 373–414 (2019)
[2] Berger, A., Scott, R., Strang, G.: Approximate boundary conditions in the finite element method. Sympos. Math. **10**, 295–313 (1972)
[3] Brenner, Susanne C., Scott, L. Ridgway: The Mathematical Theory of Finite Element Methods, 3rd edn. Springer-Verlag (2008)
[4] Chandrasekhar, Subrahmanyan: Hydrodynamic and Hydromagnetic Stability. Dover Publications, New York (1981)
[5] Choi, Haecheon, Moin, Parviz, Kim, John: Active turbulence control for drag reduction in wall-bounded flows. J. Fluid Mech. **262**, 75–110 (1994)
[6] Clopeau, Thierry, Mikelic, Andro, Robert, Raoul: On the vanishing viscosity limit for the 2D incompressible Navier-Stokes equations with the friction type boundary conditions. Nonlinearity **11**(6), 1625 (1998)
[7] Daviaud, F., Hegseth, J., Bergé, P.: Subcritical transition to turbulence in plane Couette flow. Phys. Rev. Lett. **69**(17), 2511 (1992)
[8] Lopes Filho, M.C., Nussenzveig Lopes, H.J., Planas, Gabriela: On the inviscid limit for two-dimensional incompressible flow with Navier friction condition. SIAM J. Math. Anal. **36**(4), 1130–1141 (2005)
[9] Finn, Robert: Mathematical questions relating to viscous fluid flow in an exterior domain. The Rocky Mountain Journal of Mathematics **3**(1), 107–140 (1973)
[10] Galdi, Giovanni: An introduction to the mathematical theory of the Navier-Stokes equations: Steady-state problems. Springer Science & Business Media (2011)
[11] Girault, Vivette, Sequeira, Adélia.: A well-posed problem for the exterior Stokes equations in two and three dimensions. Arch. Ration. Mech. Anal. **114**(4), 313–333 (1991)
[12] Gjerde, Ingeborg G., Scott, L. Ridgway: Nitsche's method for Navier-Stokes equations with slip boundary conditions. Mathematics of Computation **91**(334), pp.597–622: (2021)
[13] Goldstein, Sydney: Modern developments in fluid dynamics: an account of theory and experiment relating to boundary layers, turbulent motion and wakes, vol. 2. Clarendon Press (1938)
[14] Heisenberg, Werner: On Stability and Turbulence of Fluid Flows. Technical memorandums/National Advisory Committee for Aeronautics; no. 1291. U.S. Federal Government Document, Book, E-Resource (1951)
[15] Hernandez, Vicente, Roman, Jose E., Vidal, Vicente: SLEPc: A scalable and flexible toolkit for the solution of eigenvalue problems. ACM Transactions on Mathematical Software (TOMS) **31**(3), 351–362 (2005)
[16] Hoffman, Johan: Simulation of turbulent flow past bluff bodies on coarse meshes using General Galerkin methods: drag crisis and turbulent Euler solutions. Comput. Mech. **38**(4–5), 390–402 (2006)
[17] Hoffman, Johan, Jansson, Johan, Johnson, Claes: New theory of flight. J. Math. Fluid Mech. **18**(2), 219–241 (2016)
[18] Jiang, Hongyi, Cheng, Liang, Draper, Scott, An, Hongwei, Tong, Feifei: Three-dimensional direct numerical simulation of wake transitions of a circular cylinder. J. Fluid Mech. **801**, 353–391 (2016)
[19] John, Volker: Slip with friction and penetration with resistance boundary conditions for the Navier-Stokes equations-numerical tests and aspects of the implementation. J. Comput. Appl. Math. **147**(2), 287–300 (2002)
[20] Joseph, Daniel D.: Stability of Fluid Motions I, vol. 27. Springer Science & Business Media (2013)
[21] Joseph, Daniel D.: Stability of Fluid Motions II, vol. 28. Springer Science & Business Media (2013)
[22] Lin, C.C.: The Theory of Hydrodynamic Stability. Cambridge University Press, Cambridge (1955)
[23] Lions, J.L.: Quelques méthodes de résolution des problèmes aux limites non linéaires. Dunod, Paris (1969)
[24] Nakhostin, Seyedeh Mona: Investigation of transitional turbulence models to predict drag crisis for flow over spheres and cylinder. Master's thesis, University of Stavanger, Norway (2019)
[25] Neto, Chiara, Evans, Drew R., Bonaccurso, Elmar, Butt, Hans-Jürgen, Craig, Vincent S.J.: Boundary slip in Newtonian liquids: a review of experimental studies. Rep. Prog. Phys. **68**(12), 2859 (2005)
[26] Prigent, Arnaud, Grégoire, Guillaume, Chaté, Hugues, Dauchot, Olivier: Long-wavelength modulation of turbulent shear flows. Physica D **174**(1–4), 100–113 (2003)
[27] Qian, Tiezheng: Wang, Xiao-Ping, Sheng, Ping: Molecular scale contact line hydrodynamics of immiscible flows. Phys. Rev. E **68**(1), 016306 (2003)
[28] Riis, Eyvind: The Stability of Couette-flow in Non-stratified and Stratified Viscous Fluids. Universitetsforlaget, Oslo (1962)
[29] Roman, Jose E., Campos, Carmen, Romero, Eloy, Tomás, Andrés: SLEPc users manual. D. Sistemes Informatics i Computació Report No. DSIC-II/24/02, Universitat Politecnica de Valencia, Valencia, Spain (2015)
[30] Romanov, V.A.: Stability of plane-parallel Couette flow. Funct. Anal. Appl. **7**(2), 137–146 (1973)
[31] Schmid, Peter J., Henningson, Dan S.: Stability and Transition in Shear Flows. Applied Mathematical Sciences, vol. 142. Springer (2001)
[32] Scott, L. Ridgway: Introduction to Automated Modeling with FEniCS. Computational Modeling Initiative, 2018
[33] Scott, L. Ridgway: Kinetic energy flow instability with application to Couette flow. Research Report UC/CS TR-2020-07, Dept. Comp. Sci., Univ. Chicago (2020)
[34] Serrin, James: On the stability of viscous fluid motions. Arch. Ration. Mech. Anal. **3**(1), 1–13 (1959)
[35] Stenberg, Rolf: On some techniques for approximating boundary conditions in the finite element method. J. Comput. Appl. Math. **63**(1–3), 139–148 (1995)

[36] Temam, Roger: Navier-Stokes equations: theory and numerical analysis, 3rd edn. North-Holland (1984)
[37] Tillmark, Nils, Alfredsson, P. Henrik: Experiments on transition in plane Couette flow. J. Fluid Mech. **235**, 89–102 (1992)
[38] Tuckerman, Laurette S., Chantry, Matthew, Barkley, Dwight: Patterns in wall-bounded shear flows. Annual Review of Fluid Mechanics, 52 (2020)
[39] Wang, Lizhen, Xin, Zhouping, Zang, Aibin: Vanishing viscous limits for 3D Navier-Stokes equations with a Navier-slip boundary condition. J. Math. Fluid Mech. **14**(4), 791–825 (2012)
[40] Wang, Xiao-Ping, Wang, Ya-Guang., Xin, Zhouping: Boundary layers in incompressible Navier-Stokes equations with Navier boundary conditions for the vanishing viscosity limit. Commun. Math. Sci. **8**(4), 965–998 (2010)
[41] Winter, M., Schott, B., Massing, Andre, Wall, W.A.: A Nitsche cut finite element method for the Oseen problem with general Navier boundary conditions. Comput. Methods Appl. Mech. Eng. **330**, 220–252 (2018)
[42] Wolynes, Peter G., Deutch, J.M.: Slip boundary conditions and the hydrodynamic effect on diffusion controlled reactions. J. Chem. Phys. **65**(1), 450–454 (1976)
[43] Zdravkovich, Momchilo M.: Flow around circular cylinders: Volume 1: Fundamentals. Oxford University Press (1997)
[44] Zdravkovich, Momchilo M.: Flow around circular cylinders: Volume 2: Applications. Oxford University Press (1997)

L. Ridgway Scott
University of Chicago
Chicago
United States
e-mail: ridg@uchicago.edu

Ingeborg G. Gjerde
Simula Research Laboratory
Oslo
Norway

(accepted: June 25, 2022; published online: August 27, 2022)